ACS Photonics

pubs.acs.org/journal/apchd5

Perspective

# Opportunities and Challenges for Large-Scale Phase-Change Material Integrated Electro-Photonics

Rui Chen, Zhuoran Fang, Forrest Miller, Hannah Rarick, Johannes E. Fröch, and Arka Majumdar*

Cite This: https://doi.org/10.1021/acsphotonics.2c00976

Read Online

ACCESS | Metrics & More | Article Recommendations

**ABSTRACT:** Programmable photonics have the potential to completely transform a range of emerging applications, including optical computing, optical signal processing, light detecting and ranging, and quantum applications. However, implementing energy-efficient and large-scale systems remains elusive because commonly used programmable photonic approaches are volatile and energy-hungry. Recent results on nonvolatile phase-change material (PCM) integrated photonics present a promising opportunity to create truly programmable photonics. The ability to drastically change the refractive index of the PCMs in a nonvolatile fashion allows creating programmable units with zero-static energy. By taking advantage of the electrical control, nonvolatile reconfiguration, and zero crosstalk between each unit, PCMs can enable extra large-scale integrated (ELSI) photonics. In this Perspective, we briefly review the recent progress in PCM photonics and discuss the challenges and limitations of this emerging technology. We argue that energy efficiency is a more critical parameter than the operating speed for programmable photonics, making PCMs an ideal candidate. This has the potential for a disruptive paradigm shift in the reconfigurable photonics research philosophy, as slow but energy-efficient and large index modulation can provide a better solution for ELSI photonics than fast but power-hungry, small index tuning methods. We also highlight the exciting opportunities to leverage wide bandgap PCMs for visible-wavelength applications, such as quantum photonics and optogenetics, and for rewritable photonic integrated circuits (PICs) using nanosecond pulsed lasers. The latter can dramatically reduce the fabrication cost of PICs and democratize the PIC manufacturing process for rapid prototyping.

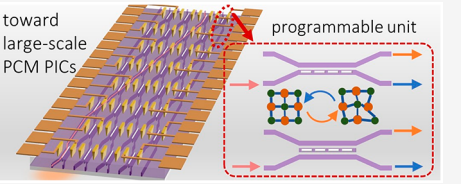


**KEYWORDS:** *phase-change materials, programmable integrated photonics, large-scale systems, laser writing*



## INTRODUCTION

While optical systems have long been considered excellent candidates for information processing,[1−4] communication,[5] and sensing,[6−8] their use in these applications remains far less common than their electronic counterparts. One fundamental limitation is the large size of the traditional free-space optical components. Thanks to the progress in nanofabrication technology and the availability of sophisticated electromagnetic simulators, it is now possible to create large-scale photonic integrated circuits (PICs) akin to electronic ICs. Many equivalents of bulky, free-space optical devices have already been developed on a chip, such as beam splitters, modulators, and lasers,[9−12] significantly shrinking the system size while retaining powerful functionalities. In various optical systems, one critical need is to reconfigure the PIC to control the light propagation by an external signal. This boils down to changing the effective refractive index in PICs. Two distinct tuning mechanisms can be identified, depending on applications: high-speed tunability or semistatic reconfiguration. High-speed tunability is desired for modulating optical signals for fast operations, exemplified by optical communication. Electro-optic[13−15] and free-carrier dispersion effects[12,16] are the leading mechanisms for high-speed tuning. In traditional PICs, most efforts have been directed toward developing high-speed modulation. In contrast, only recently have slow reconfigurations started to play an increasingly important role.

It is trivial to maintain a free-space optical setup configuration without any energy. The setup is first aligned using kinematic mounts, and once the alignment is satisfactory, the mounts are locked, with no additional energy requirement. Surprisingly, such essential nonvolatile reconfiguration appears missing in integrated photonics. For example, optical resonators fabricated in a standard foundry typically have resonance wavelengths shifted from the design wavelength, requiring additional trimming. Such trimming[17] needs a significant change in index and low energy, but the speed of change is immaterial. Similarly, display[18−20] and light detecting and ranging (LIDAR)[21−24] applications also require slow (∼100 Hz to 1 kHz) but low-energy modulation. Even for high-speed optical communications, low-speed reconfiguration plays an important role to stabilize the ring resonance against

Received: June 25, 2022
Revised: September 14, 2022
Accepted: September 14, 2022

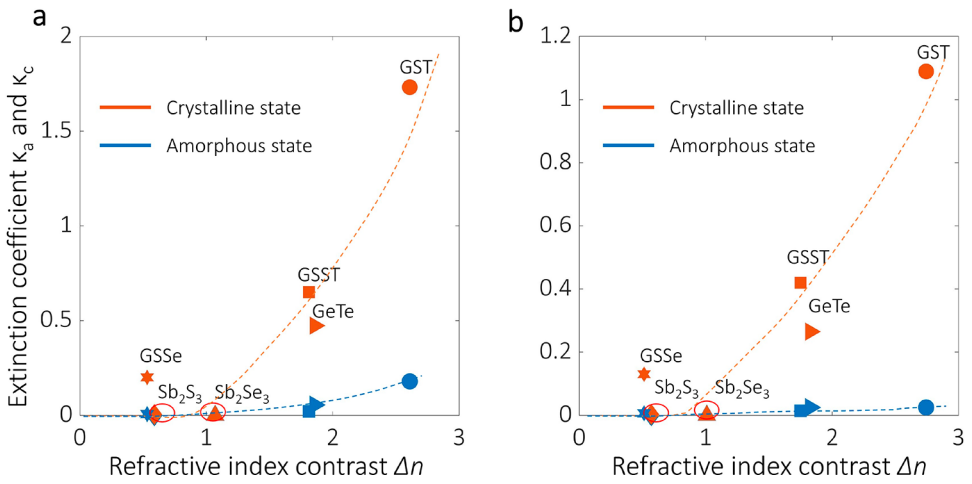


**Figure 1.** PCM optical property map at (a) 1310 and (b) 1550 nm. Materials with a small extinction coefficient or low loss are circled in red. Different optical PCMs, GST,[40] GSST,[44] $Sb_2S_3$,[42] $Sb_2Se_3$,[45] GeTe,[45] and GSSe[46] are represented with distinct symbols. The amorphous and crystalline phases are shown in blue and orange, respectively. The dashed trendlines show that the PCMs generally exhibit larger absorption losses as the refractive index contrast increases.

thermal drifts. Traditionally, slow reconfiguration in PICs is achieved either via the thermo-optic effect or microelectromechanical systems (MEMS). Thermo-optic tuning[25−29] typically requires a constant power supply of around 10 mW,[25] making them highly energy-intensive. MEMS can provide very large refractive index change,[30] but are often plagued with problems such as complicated fabrication and low yield. However, we note that these are not fundamental limitations, and MEMS-based integrated photonics is developing rapidly.[24,30−34] While mechanical actuation is electrostatic and can hold the states for some time, MEMS still requires constant refreshing (typical power of 10nW[31,35]) and thus should not be considered truly zero-static power devices.

Chalcogenide-based PCMs are a class of reconfigurable material systems heavily used in electronic memories and rewritable compact disks[36−38] (CDs), but relatively new in photonics. When undergoing a microstructural phase transition between their two stable phases, PCMs can provide a vast contrast in refractive index[39] ($\Delta n \sim 1$) and absorption.[40] This complex refractive index change enables reconfigurable photonic devices by directly integrating a thin layer of PCMs on top of photonic waveguides. The phase transition is nonvolatile, no external signal is required after switching, thus permitting truly "set and forget" type devices. In addition, PCMs are compatible with complementary metal-oxide-semiconductor (CMOS) fabrication processes by directly sputtering or evaporating onto existing PIC platforms, such as $Si_3N_4$ or silicon.[40−42] Given they are already studied and used in electronic memories, challenges and risks of high-volume manufacturing are also reasonably low.

In this Perspective, we aim to emphasize the potential of PCM technology for programmable photonic applications, particularly the urgent need for low-energy programmable units, even at the cost of slow response speed. We briefly introduce optical PCMs and discuss the state-of-the-art PCM integrated photonic devices and meta-optics. We highlight current limitations and challenges of PCM-integrated photonics, namely high optical loss, binary modulation, low endurance, and difficulty identifying accurate phase change conditions. We propose potential solutions to these challenges, outlining several future research directions. Then, we discuss the prospects of PCM devices in the visible wavelengths and their utility for quantum photonics and optogenetics. Finally, we propose creating rewritable PICs using wide bandgap PCMs, akin to rewritable CDs. With low-cost nanosecond (ns) lasers, this approach does not require a sophisticated nanofabrication facility or expensive femtosecond (fs) lasers, hence, can potentially democratize PIC fabrication for rapid prototyping.

## REVIEW OF PHASE-CHANGE MATERIAL PHOTONICS

PCMs have two stable structural phases in ambient environments: amorphous (a-PCM) and crystalline (c-PCM). The optical properties of these two states are drastically different. Therefore, by switching between them, the photonic device functionality can be changed. Notably, these two states can be reversibly switched with proper thermal pulses. In general, to change a PCM from the crystalline to the amorphous state, the PCM needs to be heated above its melting temperature $T_m$ and quenched (cooled down with rates higher than $10^9$ K·s$^{-1}$[43]). To change from amorphous to crystalline state requires heating the PCM above the glass transition temperature $T_g$, but below $T_m$. The temperature must be held for a long time (hundreds of ns or longer) to allow crystal nucleation and growth.

We compare different PCMs for three crucial material properties in Figure 1 and identify a trade-off between larger index contrast $\Delta n$ and increasing loss. For most photonic applications, we need high refractive index contrast $\Delta n$ but low material absorption ($\kappa_a$ for amorphous and $\kappa_c$ for crystalline). $Ge_2Sb_2Te_5$ (GST), one of the most heavily investigated PCMs, is especially suitable for amplitude modulation in the near-infrared (NIR) or midwave infrared (MWIR) wavelengths thanks to the drastic material loss contrast and negligible loss in the amorphous state. On the other hand, emerging transparent PCMs in the NIR, such as $Sb_2Se_3$ and $Sb_2S_3$, are excellent candidates for phase-only modulation, because of the drastic index contrast and near zero absorption loss in both phases.

To understand how material properties can determine the appropriate application, we define three optical figures of merit (FOM): (1) the refractive index change over the loss in the


https://doi.org/10.1021/acsphotonics.2c00976
ACS Photonics XXXX, XXX, XXX−XXX

Table 1. FOM for Different PCMs in 640 and 1550 nm

| | 640 nm | | | | | | 1550 nm | | | | | |
|---|---|---|---|---|---|---|---|---|---|---|---|---|
| | GST | GSST | $Sb_2S_3$ | $Sb_2Se_3$ | GeTe | GSSe | GST | GSST | $Sb_2S_3$ | $Sb_2Se_3$ | GeTe | GSSe |
| FOM1 | 0.10 | 0.77 | ∞ | 1.95 | 1.26 | 0.03 | 109.72 | 116.73 | ∞ | ∞ | 73.12 | 78.92 |
| FOM2 | 0.04 | 0.24 | **3.05** | 0.77 | 0.47 | 0.01 | 2.52 | 4.17 | 190.33 | ∞ | 6.90 | 3.95 |
| FOM3 | 2.47 | 3.18 | ∞ | 2.53 | 2.67 | 2.32 | 43.56 | 28.00 | ∞ | ∞ | 10.60 | 20 |

amorphous state $\left(\mathrm{FOM}_1 = \frac{\Delta n}{\kappa_a}\right)$, (2) the refractive index change over the loss in the crystalline state $\left(\mathrm{FOM}_2 = \frac{\Delta n}{\kappa_c}\right)$ and (3) the loss ratio between the phases $\left(\mathrm{FOM}_3 = \frac{\kappa_c}{\kappa_a}\right)$. Phase-only modulation ideally requires zero loss. Since crystalline state loss is generally higher than amorphous, $\mathrm{FOM}_2$ is suitable for assessing the worst-case insertion loss and phase tunability of the device. For amplitude modulation applications, $\mathrm{FOM}_3$ can be used to evaluate the trade-off between extinction ratio and insertion loss. For some devices, for example, nonvolatile beam splitters,[47−49] it is possible to mitigate the material loss in one of the phases by engineering device geometry. In such cases, $\mathrm{FOM}_1$ should be considered. Table 1 lists three FOM for various PCMs in the visible and telecommunication wavelengths, with bold highlighting the highest.

PCMs have already been widely used in electronics, specifically for memory applications,[50] and was first proposed as optical memories around 10 years ago.[51] Since then, tremendous efforts have been made in integrating PCMs into nanophotonics,[41,52] as shown in Figure 2. Using fast pulsed lasers (typically fs-lasers[53]), the PCMs can be switched between their crystalline, amorphous, or mixed states. Different PCM states then represent distinct bits in optical intensity. Recent works have demonstrated reliable multibit operations, large capacity, and reliability.[52,54,55] Exploiting the reliable multibit operation, researchers also used PCMs to realize neuromorphic optical computing,[29,56−60] potentially overcoming the von Neumann bottleneck in modern computer architectures. Other than applications in integrated photonics, recent years have also seen significant advancements in using PCMs for active meta-optics.[53,61−69] Meta-optics can implement arbitrary phase profiles through engineering subwavelength scale scatterers (or meta-atoms). By incorporating PCMs in these meta-atoms, the phase profile can change significantly once the microstructural phase is switched. Such active tuning capability can enable many demanding applications, for example, varifocal lens,[66,70−73] beam steering,[23,74] spatial light modulator,[75−77] and tunable holography.[78,79]

While remarkable progress has been made in optically switched PCMs, the electrical tuning for photonic devices is still in its early stage (the first work was reported only five years back[84]), despite the promised scalability of electrical control. Early works reported limited cyclability (around 10 cycles)[84] and low optical contrast (less than 1 dB).[82] Recently, high endurance (over half a million cycles[85]) and large contrast switching (more than 10 dB contrast) have been achieved using external heaters[45,83,85,86] with high-quality encapsulation.

There are predominantly two types of electrical heaters: (1) doped intrinsic semiconductor, such as silicon, on which the PICs are fabricated;[45,83,87] and (2) extrinsic heaters, such as metal,[85] graphene,[88,89] indium-doped tin oxide (ITO),[84,86] or fluorine-doped tin oxide (FTO).[90] A detailed simulation study of different heaters revealed that graphene heaters are much more electrical energy-efficient than doped semiconductors (such as PIN diode-based silicon heaters) or ITO heaters,[91] primarily because of graphene's much smaller active volume. On the other hand, PIN silicon heaters have a better heating efficiency than metal heaters[92] because the latter must be placed far from optical modes to avoid high absorption loss, reducing the thermal efficiency and optical contrast.

Optical amplitude switches[83,85,86] and phase shifters[45] are demonstrated with electrical control using doped silicon heaters. Additionally, electrically controlled tunable 2 × 2 beam splitters switching between cross and bar ports over more than 2800 cycles have been reported with GST and PIN heaters.[49] These integrated photonic devices constitute fundamental building blocks for large-scale PCM PICs. Electrically switchable meta-optics were also shown with reversible reconfigurability.[62−64] For a more in-depth discussion on PCM-based nanophotonics, we encourage the readers to refer to other review articles.[93−95]

## CHALLENGES AND OPPORTUNITIES

Despite impressive progress, several limitations and challenges exist in PCM-integrated photonics, including high optical loss of traditional PCMs, unreliable multilevel operation with electrical control, low endurance, and difficulty identifying accurate phase transition conditions. This section discusses these challenges and a few potential opportunities to mitigate them.

**High Loss of Traditional PCMs.** The high material loss of traditional PCMs, for example, GST,[40,41,83] GeTe,[45] GSST,[44] and GSSe,[85] can introduce extra device insertion loss. Deposited on top of $Si_3N_4$ or silicon waveguides, PCMs provide strong reconfigurability. However, close to the optical mode, they also induce significant optical absorption, especially in crystalline phases. Moreover, nonuniform PCM deposition, and mode mismatch at PCM interfaces can cause additional scattering loss.[45] Physically separating the PCM further from the waveguide can reduce the loss at the price of a lower refractive index contrast. Such optical loss limits applications to direct intensity modulation, although generally phase-only modulation is desired. For example, a well-known way to switch between different optical paths is to use a Mach−Zehnder Interferometer (MZI).[28,96,97] On a stardard 220 nm silicon-on-insulator (SOI) platform, using 20 nm GST in one MZI arm to modulate the phase by $\pi$ introduces ∼23 dB excess loss[49] in the crystalline state. This high excess loss drastically attenuates the signal in that arm, making the interference imperfect and reducing the extinction ratio.

To mitigate the high loss in the crystalline GST/GSST for low-loss applications, a three-waveguide device geometry (Figure 3d) was conceptualized.[47−49,98] In this scheme, only the middle waveguide is deposited with PCMs, and is purposefully phase matched with other two bare silicon waveguides when the PCM is in the amorphous state.


https://doi.org/10.1021/acsphotonics.2c00976
ACS Photonics XXXX, XXX, XXX−XXX

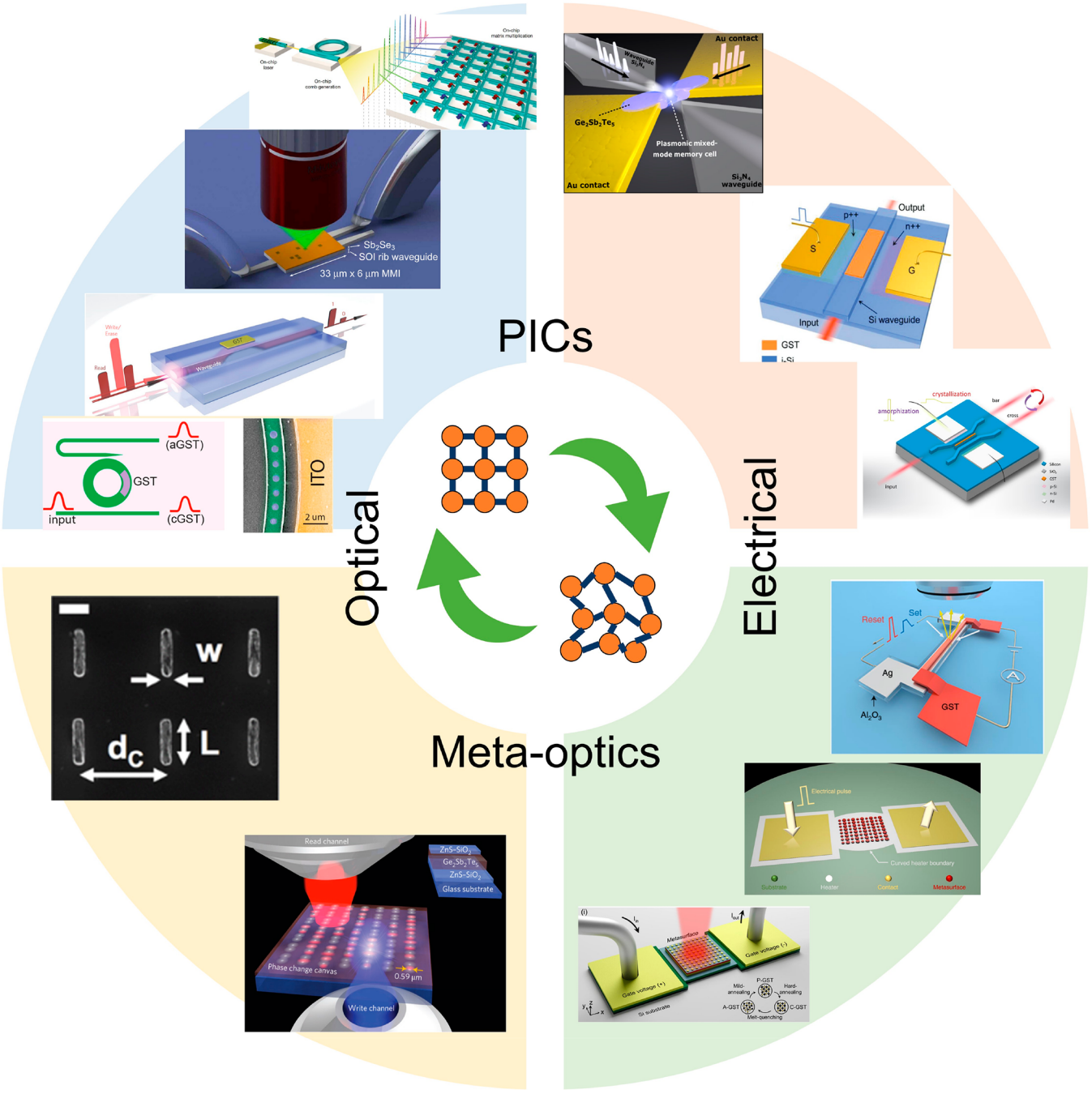


**Figure 2.** PCM-based reconfigurable integrated photonics (top)[49,52,56,80−83] and meta-optics (bottom)[53,61−64] with optical (left) or electrical (right) controls. The device functionality depends on the material phase of the PCM. In optically controlled devices, laser pulses are absorbed to heat the PCM and trigger a phase transition. This approach does not introduce any extra loss. Optically controlled PIC devices (top left, from top to bottom) have shown a wide range of applications ranging from optical neural networks[56] (Reprinted with permission from ref 56. Copyright 2021 Springer Nature), laser reconfigurable integrated photonic switches[81] (Reprinted with permission from ref 81. Copyright 2021 AAAS https://creativecommons.org/licenses/by/4.0/), multilevel all-optical integrated photonic memory[52] (Reprinted with permission from ref 52. Copyright 2015 Springer Nature), and low-loss optical switches[80] (Reprinted with permission from ref 80. Copyright 2019 American Chemical Society). In the meta-optics platform, laser-induced phase transition were also exploited for resonance tuning[61] (Reprinted with permission from ref 61. Copyright 2013 American Chemical Society), and reconfigurable metasurfaces[53] (Reprinted with permission from ref 53. Copyright 2016 Springer Nature). However, complex optical alignment is generally required, limiting the optical approach to only small-scale applications. A more scalable approach is via electrical control. Short electrical pulses are sent to on-chip heaters to generate heat and subsequently actuate the phase transition. Plasmonic device with electrical and optical dual functionality[82] (Reprinted with permission from ref 82. Copyright 2019 AAAS https://creativecommons.org/licenses/by/4.0/), doped silicon-based waveguide switch[83] (Reprinted with permission from ref 83. Copyright 2020 Wiley-VCH), and 2 × 2 programmable units[49] (Reprinted with permission from ref 49. Copyright 2022 American Chemical Society) have been demonstrated as building blocks for PCM PICs. Electrically controlled nanoantenna/metasurfaces that can tune the resonance frequency and thereby the transmission or optical beam angles have also been realized by external heaters[62−64] (Reprinted with permission from ref 62. Copyright 2022 Springer Nature https://creativecommons.org/licenses/by/4.0/; Reprinted with permission from refs 63 and 64. Copyright 2021 Springer Nature).


https://doi.org/10.1021/acsphotonics.2c00976
ACS Photonics XXXX, XXX, XXX−XXX

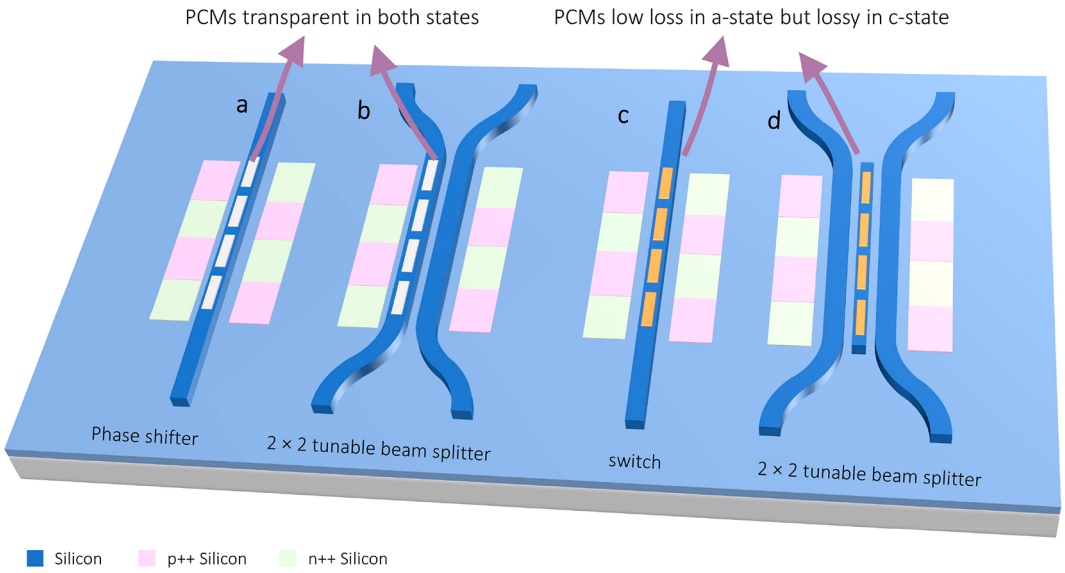


**Figure 3.** Quasi-continuously programmable phase shifters, photonic switches, and beam splitters with PCMs and PIN diode-based doped silicon microheaters on a SOI platform. (a, b) A phase shifter and a tunable beam splitter using transparent PCMs; (c, d) An amplitude switch and a tunable beam splitter using PCMs absorptive in the crystalline phase but low loss in the amorphous phase. (a) The phase of light is changed due to the PCM refractive index difference between two states. (b) Upon PCM phase transition, the coupling strength between two waveguides is changed, and the splitting ratio changes. (c) Light is switched on and off, harnessing the PCM loss difference. (d) The middle waveguide is phase matched with the other two waveguides when the PCM is in the amorphous state. In the crystalline state, the light will not be coupled to the lossy c-PCM due to the large refractive index mismatch, and the high crystalline material loss is effectively mitigated.

Therefore, light can couple to the cross output port for a-PCM. Once the PCM is switched to the crystalline phase, a large effective index mismatch significantly reduces the coupling, so the light directly transmits through the bar port and barely interacts with the lossy c-PCM, hence, bypassing the high loss. However, we note that this geometry only works for PCMs transparent in the amorphous state and requires a significant refractive index contrast. A more promising solution is to use wide bandgap PCMs, which are transparent in both phases and introduce negligible excess losses after deposited on waveguides (Figure 3). Specifically, two classes of PCMs, $Sb_2Se_3$ and $Sb_2S_3$,[39,99] have very low material absorption loss ($\kappa_a \approx 0$, $\kappa_c < 0.005$) in the telecommunication wavelength range (near 1310 and 1550 nm) due to their wide bandgap. The extra scattering loss due to mode mismatch could be relaxed by patterning the PCM into a taper shape.[45]

**Reliable Multilevel Operation with Electrical Control.** Reliable multilevel operation is difficult to achieve with electrical control, due to PCMs' stochastic nature.[100] This means that only two states (complete amorphous or crystalline phase) can be reliably produced. While using a fs-pulsed laser, reliable multilevel operations[40,52,54,55,57] have been reported, electrical control of intermediate states remains unreliable.[49] Specifically, each time an amorphization event is triggered, the stochastic melt-quench process results in a slightly different amorphous state. It then leads to significant distinctions in the subsequent long-range nucleation and growth process, hence, the PCM ends up with a stochastic partial crystalline phase.[100]

Electrically controlled PCM waveguide switches with a reliable multilevel operation were demonstrated recently using segmented heaters for both phase-only[45] and amplitude modulation.[85] Here we propose a similar scheme[85] using multiple PIN silicon heaters, as shown in Figure 3a,c. Each heater separately controls a short PCM patch in a binary but reliable manner. The device then performs reliable multilevel operation by programming the states of all PCM patches individually.

Furthermore, beam splitters with quasi-continuously tunable splitting ratios, an essential component in many PICs, can be fabricated using this similar idea (Figure 3b,d). Traditionally, such tunable beam splitters are realized in an MZI configuration, which may require active lengths exceeding 100 $\mu$m.[26,28,96,97,101] The length of the phase shifter in an MZI is given by $\sim \lambda/2\Delta n_{eff}$, with $\lambda$ being the wavelength and $\Delta n_{eff}$ being the effective index change. As $\Delta n_{eff}$ is generally small using traditional modulation methods, the phase shifter is long. Additionally, two fixed beam splitters add considerable footprint (for example, ~36 $\mu$m in ref 96), but do not contribute to the active tuning. In contrast, the PCM device footprint was shown significantly reduced to ~30 $\mu$m,[48] further improving the PIC's integration density. As conceptualized in Figure 3b, quasi-continuously programmable beam splitters are realized by placing low-loss PCM directly on one of two waveguides to form an asymmetric directional coupler,[102] and controlling with segmented heaters. With lossy PCMs, however, additional design considerations are necessary to mitigate material loss, such as adapting a three-waveguide geometry (Figure 3d), as explained earlier.

In all these devices, the central design principle is to change the coupling between waveguides by switching the PCM phase. The typical design procedure[47−49,102,103] starts with picking a PCM thickness and performing optical mode simulations of the directional couplers using an electromagnetic field solver. One can then obtain the coupling length as $L_{couple} = \lambda/2(n_e - n_o)$, with $\lambda$ being wavelength and $n_e$ and $n_o$ being the effective index of the even and odd supermode of coupled waveguides, respectively. Then, by optimizing the waveguides gap and PCM thickness, a tunable beam splitter is designed.[102]


https://doi.org/10.1021/acsphotonics.2c00976
ACS Photonics XXXX, XXX, XXX−XXX

Table 2. PCM Integrated Photonic Device Performance Comparison[a]

| ref | year | PCM | structure | ER (dB) | IL (dB) | energy per switch (nJ) | footprint ($\mu$m) | optical BW (nm) | tuning method, cycles |
|---|---|---|---|---|---|---|---|---|---|
| 52 | 2015 | GST | MRR 1 × 1 | 10 | N.R. | 0.533(3.1)[d] | 1 | <1 | optical, 50 |
| 110 | 2017 | GST | MRR 1 × 1 | 5.0 | 5.1/4.3[b] | 0.19(17.1)[d] | 60 | <1 | optical, 1000 |
| 80 | 2019 | GST | MRR 1 × 2 | 14 | 0.75/0.46[b] | 0.25(11)[d] | 25 | <1 | optical, N.R. |
| 81 | 2021 | GST | MZI 2 × 2 | 8.0 | 0.5 | 14 ($9.5 \times 10^5$)[d] | 43 | N.R. | optical, 600 |
| 84 | 2017 | GST | WG 1 × 1 | 1.2 | 4.8 | 20 ($7.2 \times 10^6$)[d] | 1 | >100 | electrical, 10 |
| 87 | 2019 | GST | MMI 1 × 1 | 6.5 | 7.5 | N.R. | 1 | >100 | electrical, 1500 |
| 83 | 2020 | GST | WG 1 × 1 | 5 | 1.6 | 13(715)[d] | 5 | >100 | electrical, 500 |
| 45 | 2021 | $Sb_2Se_3$ | MZI 2 × 2 | 6.5/15.0[b] | 0.3 | 176 ($3.8 \times 10^3$)[d] | 100[c] | >15[c] | electrical, 125 |
| 49 | 2022 | GST | DC 2 × 2 | 10.0 | 2.0 | 380 ($6.8 \times 10^3$)[d] | 50 | >30 | electrical, 2800 |

[a]ER: extinction ratio; IL: insertion loss; BW: bandwidth; MMI: multimode interferometer; MZI: Mach−Zehnder interferometer; MR(D)R: microring(disk) resonator; WG: waveguide; DC: directional coupler; N.R.: not reported. Note: here, only devices with reversible switching are compared. Footprint refers to the total device length. [b]For cross and bar states, respectively. [c]Estimated from figures. [d]Energy per switching event for amorphization (crystallization).

**Limited PCM Endurance.** Another important unsolved issue is the limited PCM endurance,[104] that is, how many times the PCM can be cycled through. Recent years have witnessed orders of magnitude improvement in optical PCM devices' cyclability (10 cycles[84] to half $10^6$ cycles[85] with different PCMs and heater designs, see Table 2), thanks to the development of high performance microheaters and encapsulation materials. However, the cycle number is still much lower than what has been achieved in electronic memories ($10^{12}$ cycles,[37] and potentially $10^{15}$ cycles[105] for GST). The reason might be that PCMs in electronic memories are typically shaped into tiny units of volume ($10 \times 10 \times 10$ nm$^3$),[106] whereas the size is much larger ($10\ \mu m \times 1\ \mu m \times 10$ nm)[42,49,83] in integrated photonics. Generally, a smaller PCM volume suffers less degradation from thermal reflowing issues and is also less prone to elemental segregation, which causes material failure.[80] Assuming a linear scaling with volume, we expect to achieve around $10^{10}$ cycles in photonics. We note that even $10^{10}$ cycles are insufficient for high-speed modulation. For example, a GHz modulator with an endurance of $10^{10}$ would only last 10 s!! While this is a severe limitation, $10^{10}$ cycles are sufficiently high for reconfigurable applications. Assuming a PIC/meta-optic is changed, kept for 1 s, and changed again for another application, it takes more than 300 years to complete $10^{10}$ cycles! Besides, the kept time could be much longer for many applications, such as optical computing or optical programmable gate arrays (OPGAs). Therefore, temporal response or the switching times of PCM-based programmable units are of little significance.[107]

The endurance can be enhanced with better encapsulation materials. Different encapsulation materials[104] have been used to protect the PCM from thermal reflowing and oxidation, including ITO,[52] $SiO_2$,[108] $Si_3N_4$,[108] $ZnS/SiO_2$,[53] $Al_2O_3$,[29,49,83] and others.[108] In particular, recent developments show that atomic-layer deposited $Al_2O_3$ can provide excellent protection,[29,49,83] primarily due to its highly conformal nature. Besides, further optimizing the material property may also help improve device endurance. For example, to avoid element segregation, single-element PCMs[109] may be explored. Finally, since smaller volumes of PCM are more durable,[80] patterning the PCM on a subwavelength scale[29,80] could improve device endurance. We refer readers to a recent review[104] on this topic.

**Difficulty Identifying Phase Change Conditions.** Identifying the phase transition condition is nontrivial because the amorphization condition can be close to the device damaging threshold. We consider the silicon PIN heater and GST as an example in the following. In comparison to silicon, GST has lower melting temperature $T_m$ ($T_{m,Si}$ = 1450 °C, $T_{m,GST}$ = 650 °C), thermal conductivity $k_{th}$ ($k_{th,Si}$ = 148W/m·K, $k_{th,GST}$ < 1 W/m·K), and specific heat capacity $C_p$[111] ($C_{p,Si}$ = 0.72 J/g·K, $C_{p,GST}$ = 0.2 J/g·K). A smaller thermal conductivity means that heat diffuses away slower and hence becomes more localized within the GST. A smaller specific heat capacity indicates GST requires less energy to heat up. Therefore, the low melting point $T_m$, thermal conductivity $k_{th}$, and heat capacity $C_p$ all together imply that GST is much easier to melt than silicon with the same input energy. However, in our experiments, the silicon waveguide could be damaged when applying a voltage slightly higher (~0.3 V) than the amorphization voltage. Simulations[91,92] suggest that such surprising device damage stems from local hotspots at the edge of the waveguide, due to current crowding, as the silicon thickness abruptly changes between the waveguide and partially etched slab. Moreover, the phase change condition is not universal. As the phase transition is thermally induced, any change in the substrate or the cladding requires reoptimizing the heating conditions.

Although identifying the accurate phase change conditions requires trials and errors, the conditions are reliable, once found. Therefore, the conditions must be identified on several separate testing devices before being applied on large-scale PICs. We can also further optimize the material systems to facilitate a larger amorphization window, for example, designing new PCMs with lower $T_m$, or exploring other photonic backbone materials with higher $T_m$ than silicon, such as $Si_3N_4$. Another important research direction is to optimize the heaters. For doped silicon heaters, the geometry of the doping area and the silicon waveguides can be optimized to eliminate the local hotspots. Besides, new heaters, such as graphene heaters,[89,91] should be explored to maximize heat delivery to the PCMs, easing the stringent phase change conditions and significantly improving their energy efficiency.

## OPPORTUNITIES TOWARD LARGE-SCALE SYSTEMS

The main advantage of using PCMs in large-scale systems comes from their zero-static power consumption. Here, we perform a simple calculation on the energy consumption to stress the utility of small (or zero) static energy consumption for semistatic active photonics. Let us consider a thermo-optically tunable component, which usually consumes 10 mW power.[96,97] The energy consumption to hold the system


https://doi.org/10.1021/acsphotonics.2c00976
ACS Photonics XXXX, XXX, XXX−XXX

**Table 3. State-of-the-Art PIC Systems Comparison**[a]

| ref | application | year | mechanism, platform | device IL (dB) | device ER (dB) | active length ($\mu$m) | device power (mW or mJ/switch) | # of devices | system IL (dB) | system footprint ($\mu$m × $\mu$m) |
|---|---|---|---|---|---|---|---|---|---|---|
| 114 | SF | 2016 | EO, SOI | 0.44 | 30(18)[b] | 380 | 26 | 56 | 6.7(14)[d] | 10700 × 4400 |
| 26 | OPGA | 2015 | TO, $Si_3N_4$ | N.R. | N.R. | 2100 | 250 | 9 | 1.0 | 8500 × 3500 |
| 28, 101 | OPGA | 2017 (2020) | TO, SOI | 0.6 | N.R. | 800[c] | 110 | 60 | 0–30[d] | 1500 × 2000 |
| 27 | OPGA | 2020 | TO, SOI | 0.8(9.0)[b] | 5(30)[b] | 6 | 1.6 | 128 | 2.8(9.8), 4(18)[d] | 300 × 300[c] |
| 29, 115 | ONN | 2021 (2022) | PCM, $Si_3N_4$ | 0.9(6.5)[b] | 8.5(9.5)[b] | 10 | $3.81 \times 10^{-7}$ | 4 | N.R. | N.R. |
| 96, 97 | ONN, QS | 2017 | TO, SOI | $3 \times 10^{-3}$ | 66.3 | 33[c] | 10 | 48/176 | 8.0 | 1830 × 4100[c] |
| 116 | ONN | 2019 | PCM, $Si_3N_4$ | 1.5 | 9 | 3 | $7 \times 10^{-7}$ | 4 | N.R. | 2461 × 270[c] |
| 56 | ONN | 2021 | PCM, $Si_3N_4$ | 0.4 | N.R. | 2 | $8 \times 10^{-7}$ | 16/64 | 12 | 1140 × 1416 |
| envisioned PCM systems | | | PCM, SOI/$Si_3N_4$ | 0.1 | 30 | <30 | $10^{-7}$ | >100 | <10 | 500 × 500 |

[a]ER: extinction ratio; IL: insertion loss; N.R.: not reported; SF: switching fabric; OPGA: optical programmable gate array; ONN: optical neural networks; QS: quantum simulation. Note: The device power for volatile (nonvolatile) devices is in mW (mJ/switching event). [b]For cross and bar states, respectively. [c]Estimated from figures. [d]Performance for different configurations.

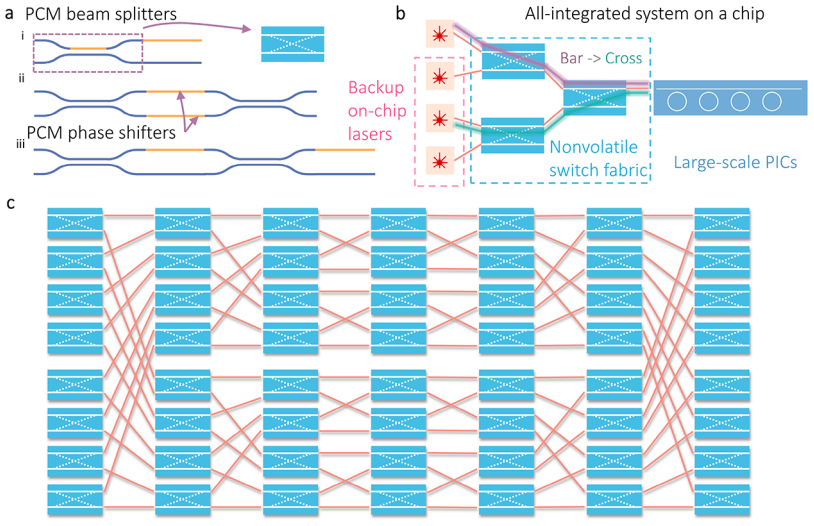


**Figure 4.** Schematic of nonvolatile arbitrary unitary transformation and switching fabrics. (a) Three schematics of programmable units for arbitrary unitary transformation based on PCMs (orange). The tunable beam splitter is boxed in purple dotted lines. (b) Proposed switching fabrics for adding optical redundancy to all-integrated systems on a chip. Because on-chip lasers are prone to failure, one can fabricate several backup lasers together. The PCM-based switching fabric in the dotted light blue box can be placed between the laser and the large-scale PICs (such as an array of ring modulators in optical transceivers). The switching fabric routes a functioning laser to the PIC using zero-static energy, akin to a free-space optomechanical setup. (c) Proposed 16 × 16 Benes-type nonblocking switching fabrics for nonvolatile signal routing. We envision all the tunable beam splitters will be programmed electrically.

configuration is thus estimated as 10 mW × 3600 s = 36 J/hour or 864 J/day. Compared with the typical energy of 1 $\mu$J (or less) to switch a PCM device, the static energy consumption is 7 orders of magnitude larger per hour per switch!!

In addition to the energy saving benefit, the weak thermo-optic effect usually leads to a very high temperature at the heater locations, resulting in thermal crosstalk. Such thermal crosstalk limits the optical component density and may cause unreliable operations. PCM devices need a relatively high thermal threshold to switch, and hence are unaffected by such thermal crosstalk. Although researchers recently developed many algorithms[101,112] to compensate for the thermal crosstalk, they require additional software and complex control circuits.

Overcoming the challenges outlined in the previous section will create opportunities to build large-scale electrically controlled PCM PICs for various applications, including quasi-arbitrary unitary transformation,[113] nonblocking switching fabrics,[114] adding redundancy to optical systems, multipurpose PICs,[26−28,101] optical neural networks,[29,56,96,115,116] and quantum simulations.[97] As an overview, Table 3 compares several state-of-the-art PICs at the device (insertion loss, extinction ratio, active region length, and power consumption) and system levels (number of devices, insertion loss, and footprint). The envisioned performances for PCM systems are listed in the last row, highlighting the advantage of compact footprint, low energy consumption and large system size. We also refer the readers to a few review articles[112,117,118] on programmable PICs.


https://doi.org/10.1021/acsphotonics.2c00976
ACS Photonics XXXX, XXX, XXX−XXX

**Quasi-Arbitrary Unitary Transformation.** Any arbitrary unitary transformation can be implemented optically using an array of programmable units consisting of a tunable beam splitter and a phase shifter.[113] Using these optical unitary transformations, we can implement matrix-vector multiplication at the heart of optical signal processing,[101,119,120] neural networks,[96] and even quantum simulation.[97] Although these systems have been demonstrated using the thermo-optic effect in the past,[28,96,97,101] the number of programmable units remains limited due to thermal crosstalk, massive energy consumption, and complex control circuit. A nonvolatile programmable unit, as shown in Figure 4a, can circumvent these problems. However, no electrically controlled PCM demonstrations currently exist in a system level due to the challenges in the previous section, such as the high loss. While the loss in PCMs can be acceptable for a single unit, these losses add up for massive arrays of devices and incur a considerable signal reduction. Additionally, the loss can be nonuniform along different paths and further limit the system performance.[47] Therefore, we must ensure an excess insertion loss of <0.1 dB and an extinction ratio of >30 dB per programmable unit for a large system, with at least ∼10 units in the critical path. This is beyond the capabilities of traditional PCMs such as GST because 20 nm thick c-GST on a standard silicon waveguide introduces an insertion loss of around 7 dB/$\mu$m.[40,83] Wide bandgap PCMs, for example, $Sb_2S_3$ and $Sb_2Se_3$,[39,99] exhibit a low insertion loss of less than 0.02 dB/$\mu$m in the same setting, reducing the loss by more than 300-fold. The $Sb_2Se_3$-based PCM phase shifters[45] demonstrate a promising approach to this application, but more work is required to further reduce the loss from 0.33 dB[45] to less than 0.1 dB and to achieve more operation levels reliably.

**Adding Optical Redundancy with Nonblocking Switching Fabric.** A large PIC may contain some critical components that are more prone to failure, and such single-device failure can incur an entirely unusable PIC. A straightforward approach to overcome this is to add several backup devices and a switching fabric, bypassing the broken device and rewiring a functional device. Figure 4b shows a proposed schematic of a fully integrated transceiver with multiple on-chip lasers and a PCM nonvolatile switching fabric. This type of switching fabric demands zero-static energy but has no switching speed requirement, rendering PCMs ideal candidates. Other switching fabrics may also be established with PCMs, such as the 16 × 16 Benes-type nonblocking switch fabric[47] (Figure 4c), which can route all input signals to corresponding output ports simultaneously. We again stress that the successful creation of such a fabric requires optimized insertion loss (<0.1 dB) and extinction ratio (>30 dB). Although this is possible in theoretical designs,[47,103] currently reported PCM programmable units (listed in Table 2) do not yet meet such stringent demands, primarily due to fabrication imperfections and residual material losses. Therefore, further research and engineering on loss reduction techniques are needed.

**Optical Neural Networks.** Deep neural networks have been an immensely promising platform for many problems, such as image recognition and classification,[121−123] natural language processing,[124−126] image-to-image translation,[127,128] artwork generation,[129] and mathematical problem solving.[130−132] With the enlarging problem space, increasingly larger neural networks are implemented, which, unfortunately, requires prohibitive amount of computational resources.

Photonics has the potential advantage of being lower loss and faster than electronics, providing power-efficient and high-speed computation. Therefore, implementing part of the artificial neural networks, especially the linear operations, using optics is a promising alternative. Recently, rudimentary deep neural networks,[96] convolutional neural networks,[29,56] reservoir networks,[133] and generative adversarial networks[59] have been implemented using photonics.

In optical neural networks (ONNs), the input vector is encoded in the phase and amplitude of the input light. The weights (matrices) are implemented by PICs using tunable devices, such as MZI or crossing meshes, as shown in Figure 5a and b, respectively. Therefore, a matrix-vector multiplication is performed by propagating the light through the PIC. Notably, once the neural networks are trained, the weights are fixed, hence a fixed PIC configuration. In other words, holding the PIC for a long time is necessary here, making PCM photonics an encouraging solution. Indeed, spiking neurosynaptic networks with self-learning capability[116] and convolutional neural networks[29,56] have already been demonstrated with GST. Nevertheless, all the ONNs mentioned above relied on optical control, complicating the laser alignment, and potentially hindering the scalability. On the contrary, electrically controlled PCM devices and electronic integrated circuits (EIC) could be packaged together,[134,135] even monolithically integrated on the same chip,[17,136] offering a higher degree of integration and flexibility. Therefore, electrically controlled PCM photonics is a promising path toward energy efficient and large-scale optical neural networks (Figure 5).

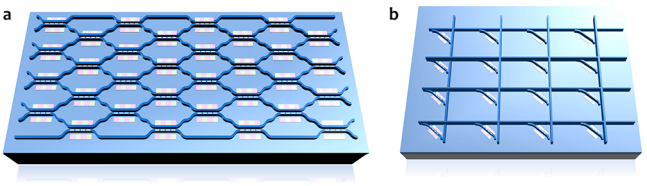


**Figure 5.** Schematic of PCM-based nonvolatile platform to perform linear operations in an optical neural network. (a) A forward matrix-vector multiplier for deep neural network based on PCM tunable beam splitters; (b) A convolutional block using a tunable attenuator.

**Nonvolatile Electro-Optical Programmable Gate Array.** PICs have been primarily worked in application-specific ways, where they are carefully designed and optimized for a particular task. However, there is an increasing interest in creating a general-purpose PIC, that is, developing optical programmable gate arrays (OPGAs),[26−28,101] an idea inspired by the electronic field-programmable gate array (FPGA). These OPGAs can be reconfigured to implement different functionalities. Each gate consists of the programmable unit described earlier (Figure 4a) and is connected in meshes,[26−28,101] such as the rectangular meshes shown in Figure 6a. The edges are PCM-based quasi-arbitrary unitary transformation unit (Figure 6b).

The resulting chip can perform various functions by appropriately programming the array (Figure 6c). The functionalities of the OPGA are optimal when each unit is nonresonant, making them applicable over a broad wavelength range. Obviously, this type of PIC does not require frequent reconfiguration. So "set-and-forget" type devices are demanding. To date, most of the demonstrated OPGAs are, however, based on thermo-optic effects,[26−28,101] consuming an enor-


https://doi.org/10.1021/acsphotonics.2c00976
ACS Photonics XXXX, XXX, XXX−XXX

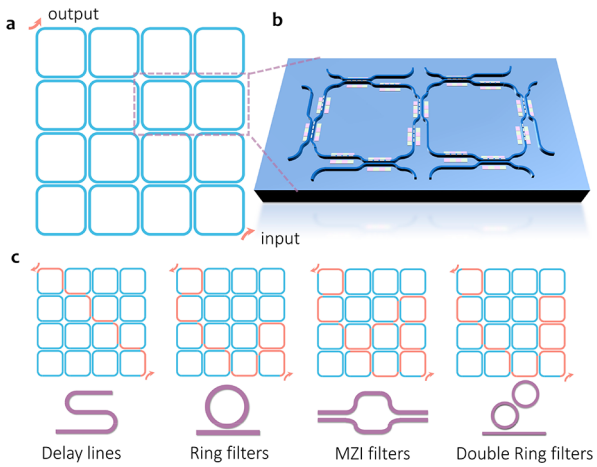


**Figure 6.** Nonvolatile programmable gate arrays based on PCMs. (a) Schematic of a nonvolatile programmable gate array in a rectangular mesh. (b) Schematic of two meshes shown in the dotted purple box. Each edge of the mesh is a programmable unit. (c) Working principles of OPGAs. The light traveling path, denoted by orange, can be changed by programming the OPGA. In this way, the OPGA can implement various functions on the same chip, such as delay lines, ring filters, MZI filters, and double ring filters.

mous amount of static energy, see Table 3. Besides, the compactness of PCM devices offers more available meshes and functionalities.[28] We see many exciting opportunities in PCM-based zero static-energy OPGAs using the wide-bandgap PCMs and the electrically controlled quasi-continuous tuning devices.

## VISIBLE PHASE-CHANGE MATERIAL PHOTONICS

While integrated photonics research was pioneered in the infrared telecommunication bands, in recent years, visible integrated photonics has generated strong interest for many applications, including optogenetics,[137] spectroscopy,[138,139] augmented reality visors,[140] and quantum optics.[141,142] Barring some rudimentary demonstrations of PCM-integrated visible photonics,[42] this field remains largely unexplored due to the narrow bandgap of traditional PCMs and ensuing strong absorption in the shorter wavelengths. For example, traditional PCMs, such as GST,[40] GSST,[44] GeTe,[45] and GSSe,[46] are very lossy at visible wavelengths in both amorphous and crystalline phases, see Table 1. $Sb_2S_3$, explored in the late 20th century for memory applications,[143] has a wide bandgap and zero loss in the amorphous state down to a wavelength of ~600 nm.[39,99] Table 1 compares different PCMs at 640 nm, and $Sb_2S_3$ shows the best performances in all three FOM. Thus, $Sb_2S_3$ is particularly suitable for visible or near-IR (>600 nm) applications, specifically for routing of single photons emitted from semiconductor color centers, such as silicon-vacancy (SiV)[141] and nitrogen-vacancy (NV)[142] centers in diamond.

The finite c-$Sb_2S_3$ loss in visible wavelength could be mitigated using ring resonators[42] or three-waveguide directional couplers[48] on a $Si_3N_4$ platform. In Figure 7a, we show the schematic of a tunable beam splitter made of $Sb_2S_3$ on $Si_3N_4$, where the state of $Sb_2S_3$ can be switched by external heaters such as ITO, graphene, or tungsten. Another possible approach can be to integrate $Sb_2S_3$ on wide bandgap semiconductors, such as gallium phosphide,[144] which can be directly doped to create a heater, similar to doped silicon heaters in silicon photonics.[45,49,83]

One promising application of this wide bandgap PCM could be to create a visible switching fabric to connect functional quantum devices and route single photons on-chip. Quantum devices, such as single-photon sources, on-chip superconducting detectors, or quantum frequency converters, have a moderate to low success probability, which diminishes as many such devices are hardwired. One way to circumvent this issue is the "pick-and-place" technique, where precharacterized functional devices are picked up and placed on a previously defined PIC.[145,146] However, the scalability of such approaches may be limited. In contrast, by using a nonvolatile switching fabric, we can connect selected functional quantum devices on-chip.

The emission wavelengths of most solid-state single-photon sources and the atomic transitions of alkali and alkaline earth metals used in quantum memory are in the visible or near-infrared wavelength range. By using nonvolatile and wide bandgap $Sb_2S_3$, we can realize low-loss reconfigurable visible

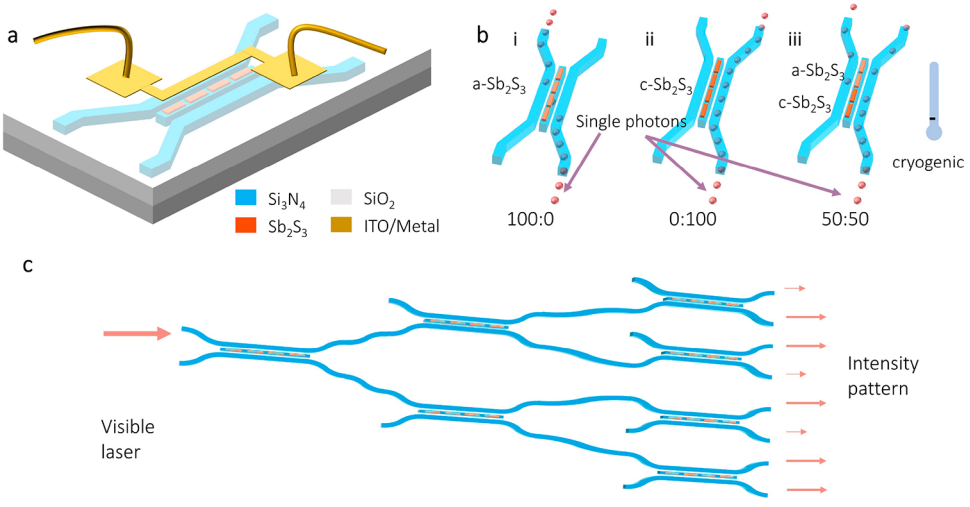


**Figure 7.** Nonvolatile active photonics in the visible employing emerging wide bandgap PCM $Sb_2S_3$. (a) Schematic of an electrically tunable 2 × 2 tunable beam splitter in the visible spectrum. (b) Schematics for switching single photons for quantum applications in a cryogenic temperature, achieving on-demand splitting ratios. (c) Concept of a nonvolatile switch for optogenetic applications.[137]


https://doi.org/10.1021/acsphotonics.2c00976
ACS Photonics XXXX, XXX, XXX−XXX

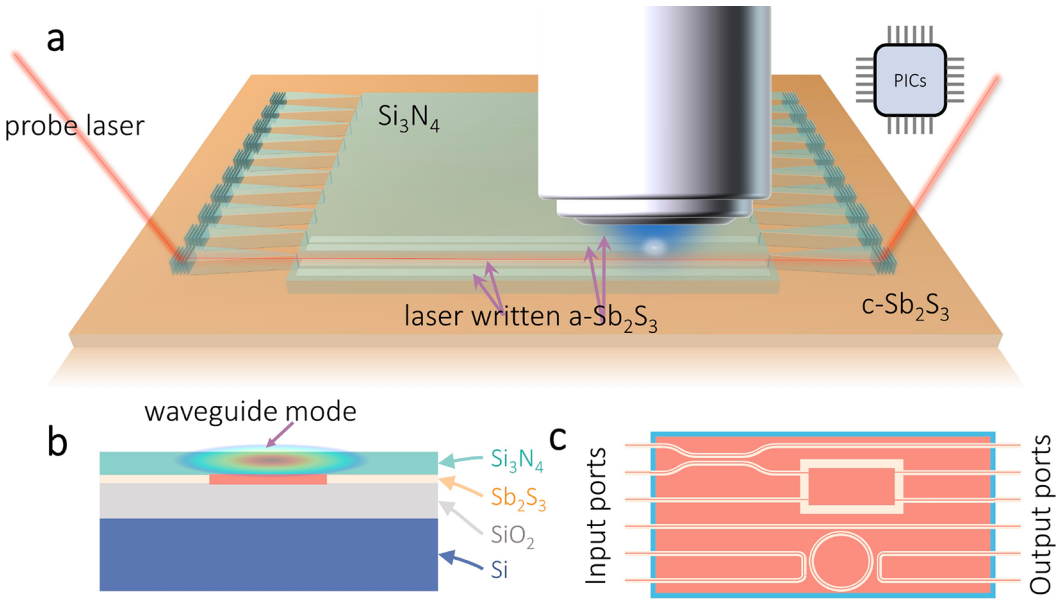


**Figure 8.** Lithography-free rewritable PICs using ns-lasers and PCMs. (a) Proposed laser written PIC in wide bandgap PCM ($Sb_2Se_3$ or $Sb_2S_3$). Optical waveguides are defined by two $Sb_2S_3$ strips (in white, pointed by purple arrows) amorphized by a focused ns blue pulse laser and leaving the center portion crystalline. Prefabricated grating couplers can provide the input/output interfaces. The photonic circuitry is fully reprogrammable and only limited by material loss and laser writing resolution. (b) An example material stack consists of a silicon substrate, a few microns of silicon dioxide, tens of nanometers $Sb_2S_3$, and several hundred nanometers of $Si_3N_4$ cladding. When a strip of $Sb_2S_3$ is switched from crystalline (dark orange) to amorphous (light orange) phase, a waveguide mode is confined, located mainly in the $Si_3N_4$ layer to reduce loss. (c) Concept of photonic devices beyond waveguides that can be implemented in this platform, such as directional couplers, multimode interferometers, and ring resonators. Here light and dark orange colors indicate a and c-$Sb_2S_3$, respectively.

PICs. Figure 7b shows a $Sb_2S_3$-based nonvolatile switch that can control single photon paths. Additionally, unlike thermo-optic or free-carrier dispersion effects, PCMs can be efficiently tuned even at cryogenic temperatures. The relatively low energy density for switching PCMs[45,83] will not provide a considerable energy burden to tune them inside a cryostat. Alternatively, these devices can even be programmed at room temperature before putting in a cryogenic environment. We note that, for quantum photonics, the loss per programmable unit needs to be even lower than what is required for classical applications; specifically, we estimate the required loss <0.01 dB per unit.[97]

$Sb_2S_3$ can also enable biological applications. For example, Figure 7c shows the concept of a switching fabric that can be used in light delivery for optogenetics,[137] where by simultaneously stimulating selective regions in the brain, collective neural functions can be studied. PCMs render a much safer solution than the previously reported thermal tuning.[137] Moreover, the programming process could even happen before placing the probe inside the brain, mitigating potential heat-related harm.

## LASER REWRITEABLE PHASE-CHANGE MATERIAL INTEGRATED PHOTONICS

Lithography-free laser writing[147−152] is becoming increasingly popular in integrated photonics as it provides significant flexibility for rapid prototyping and on-demand designs. However, traditional laser writing techniques in glass require costly fs-pulse lasers. Additionally, they only induce miniscule material refractive index change ($\Delta n \approx 0.02$) and are limited to large waveguides (~10 $\mu$m wide). Moreover, the writing process is generally irreversible.[147]

As the dominant optical data storage materials, PCMs have been reversibly switched with ns-lasers in commercial CD writers.[50] Compared to fs-lasers, ns-lasers are significantly cheaper. In CDs, data is recorded by amorphizing PCM strips and erased with crystallization pulses. The minimal feature size of a commercial Blue-Ray CD is as tiny as ~150 nm.[50] For integrated photonics, one major obstacle was, again, the high loss of traditional PCMs. However, the loss can be overcome by exploiting emerging wide bandgap PCMs and designing low-loss waveguides.

Laser-written PCM photonic devices have already been demonstrated for meta-optics[53] and tunable beam splitters,[81] which were limited to a single device. In Figure 8a, we envision expanding this technology to create large-scale rewritable PICs. A carefully designed material stack builds the canvas for a rewritable photonic architecture. An example material stack (Figure 8b) includes tens of nanometer thick c-$Sb_2S_3$ on a few microns thick layer $SiO_2$, cladded with a few hundred nanometers of $Si_3N_4$. In this configuration, the optical guided mode is mainly confined within the $Si_3N_4$ cladding layer to ensure low absorptive loss from c-$Sb_2S_3$. The relatively thin layer of $Sb_2S_3$ and $Si_3N_4$ also allows $Sb_2S_3$ to be switched entirely and reversibly with high spatial resolution from the top. A ns-pulsed laser at a shorter wavelength (e.g., 450 nm), similar to a CD-writer, selectively "patterns" (i.e., amorphizes) the PCM. The probe laser at IR wavelength is guided by the total internal reflection at the interface of patterned a-PCM and unpatterned c-PCM. As illustrated in Figure 8c, many other functionalities can potentially be implemented beyond simply routing through an optical waveguide, such as ring resonators, directional couplers, and multimode interferometers. The same chip/wafer can be switched back to its


https://doi.org/10.1021/acsphotonics.2c00976
ACS Photonics XXXX, XXX, XXX−XXX

crystalline state by rapid thermal annealing[41] and rewritten again.

Compared with previously reported multipurpose PICs,[26−28,101] the achievable functions in this rewritable PICs are only limited by the laser writing resolution and the material losses, and not by the discrete meshes. Thus, such laser-writable PCM can be considered as programmable PICs at the most extreme level, where each pixel can be programmed. Beside, this process can be much faster, and more cost-effective for simple designs and rapid prototyping than fabricating a PIC in a nanofabrication facility. However, we note that the proposed laser writing approach is unlikely to entirely replace traditional nanofabrication. The limited spatial resolution of laser writing and repeatability of PCM switching will limit possible applications. Instead, it should be considered as a new path: a fast, cheap, and rewritable platform for devices with large feature sizes.

## CONCLUSION

In summary, PCM-based photonics provides a promising approach to nonvolatile, energy efficient and large-scale PIC systems. For semistatic applications, the zero-static-energy consumption in PCM is highly desirable. However, to achieve a large-scale electrically controlled PCM system, some challenges remain to be carefully addressed. We have outlined these challenges and prescribed several future research avenues to tackle them. We also identified several promising applications if these challenges can be successfully mitigated. We pointed out that the emerging wide bandgap PCM $Sb_2S_3$ can potentially enable visible programmable PICs with applications in optogenetics and quantum photonics. Beyond that, we lastly envision a rewritable PIC platform using nanosecond pulsed lasers and wide bandgap PCMs, drastically reducing the fabrication cost.

## AUTHOR INFORMATION


### Corresponding Author

**Arka Majumdar** − *Department of Electrical and Computer Engineering and Department of Physics, University of Washington, Seattle, Washington 98195, United States;* orcid.org/0000-0003-0917-590X; Email: arka@uw.edu

### Authors

**Rui Chen** − *Department of Electrical and Computer Engineering, University of Washington, Seattle, Washington 98195, United States;* orcid.org/0000-0001-8492-729X

**Zhuoran Fang** − *Department of Electrical and Computer Engineering, University of Washington, Seattle, Washington 98195, United States;* orcid.org/0000-0001-8724-6633

**Forrest Miller** − *Department of Electrical and Computer Engineering, University of Washington, Seattle, Washington 98195, United States*

**Hannah Rarick** − *Department of Physics, University of Washington, Seattle, Washington 98195, United States*

**Johannes E. Fröch** − *Department of Electrical and Computer Engineering, University of Washington, Seattle, Washington 98195, United States*

Complete contact information is available at: https://pubs.acs.org/10.1021/acsphotonics.2c00976



### Funding

The research reported here is funded by National Science Foundation (NSF-2003509), ONR-YIP Award, DARPA-YFA Award, DRAPER Laboratories, and Intel.


### Notes

The authors declare no competing financial interest.

## REFERENCES


(1) Sawchuk, A. A.; Strand, T. C. Digital Optical Computing. *Proc. IEEE* **1984**, *72* (7), 758−779.

(2) Ambs, P. Optical Computing: A 60-Year Adventure. *Adv. Opt. Technol.* **2010**, *2010*, 372652.

(3) Johnson, K. M.; Handschy, M. A.; Pagano-Stauffer, L. A. Optical Computing And Image Processing With Ferroelectric Liquid Crystals. *Opt. Eng.* **1987**, *26* (5), 385−391.

(4) Caulfield, H. J.; Kinser, J.; Rogers, S. K. Optical Neural Networks. *Proc. IEEE* **1989**, *77* (10), 1573−1583.

(5) Gagliardi, R. M.; Karp, S.*Optical Communications*; Wiley-Interscience, 1976.

(6) Lee, Y.-S.; Joo, B.-S.; Choi, N.-J.; Lim, J.-O.; Huh, J.-S.; Lee, D.-D. Visible Optical Sensing of Ammonia Based on Polyaniline Film. *Sens. Actuators B Chem.* **2003**, *93* (1), 148−152.

(7) Singh, V.; Lin, P. T.; Patel, N.; Lin, H.; Li, L.; Zou, Y.; Deng, F.; Ni, C.; Hu, J.; Giammarco, J.; Soliani, A. P.; Zdyrko, B.; Luzinov, I.; Novak, S.; Novak, J.; Wachtel, P.; Danto, S.; Musgraves, J. D.; Richardson, K.; Kimerling, L. C.; Agarwal, A. M. Mid-Infrared Materials and Devices on a Si Platform for Optical Sensing. *Sci. Technol. Adv. Mater.* **2014**, *15* (1), 014603.

(8) Fallon, R. W.; Zhang, L.; Everall, L. A.; Williams, J. A. R.; Bennion, I. All-Fibre Optical Sensing System: Bragg Grating Sensor Interrogated by a Long-Period Grating. *Meas. Sci. Technol.* **1998**, *9* (12), 1969−1973.

(9) Dai, D.; Bauters, J.; Bowers, J. E. Passive Technologies for Future Large-Scale Photonic Integrated Circuits on Silicon: Polarization Handling, Light Non-Reciprocity and Loss Reduction. *Light Sci. Appl.* **2012**, *1* (3), e1.

(10) Kang, Y.; Liu, H.-D.; Morse, M.; Paniccia, M. J.; Zadka, M.; Litski, S.; Sarid, G.; Pauchard, A.; Kuo, Y.-H.; Chen, H.-W.; Zaoui, W. S.; Bowers, J. E.; Beling, A.; McIntosh, D. C.; Zheng, X.; Campbell, J. C. Monolithic Germanium/Silicon Avalanche Photodiodes with 340 GHz Gain−Bandwidth Product. *Nat. Photonics* **2009**, *3* (1), 59−63.

(11) Liang, D.; Bowers, J. E. Recent Progress in Lasers on Silicon. *Nat. Photonics* **2010**, *4* (8), 511−517.

(12) Xu, Q.; Schmidt, B.; Pradhan, S.; Lipson, M. Micrometre-Scale Silicon Electro-Optic Modulator. *Nature* **2005**, *435* (7040), 325−327.

(13) Block, B. A.; Younkin, T. R.; Davids, P. S.; Reshotko, M. R.; Chang, P.; Polishak, B. M.; Huang, S.; Luo, J.; Jen, A. K. Y. Electro-Optic Polymer Cladding Ring Resonator Modulators. *Opt. Express, OE* **2008**, *16* (22), 18326−18333.

(14) Lu, G. W.; Hong, J.; Qiu, F.; Spring, A. M.; Kashino, T.; Oshima, J.; Ozawa, M.; Nawata, H.; Yokoyama, S. High-Temperature-Resistant Silicon-Polymer Hybrid Modulator Operating at up to 200 Gbit S−1 for Energy-Efficient Datacentres and Harsh-Environment Applications. *Nat. Commun.* **2020**, *11* (1), 4224.

(15) Wang, C.; Zhang, M.; Chen, X.; Bertrand, M.; Shams-Ansari, A.; Chandrasekhar, S.; Winzer, P.; Lončar, M. Integrated Lithium Niobate Electro-Optic Modulators Operating at CMOS-Compatible Voltages. *Nature* **2018**, *562* (7725), 101−104.

(16) Qiu, C.; Gao, W.; Soref, R.; Robinson, J. T.; Xu, Q. Reconfigurable Electro-Optical Directed-Logic Circuit Using Carrier-Depletion Micro-Ring Resonators. *Opt. Lett., OL* **2014**, *39* (24), 6767−6770.

(17) Atabaki, A. H.; Moazeni, S.; Pavanello, F.; Gevorgyan, H.; Notaros, J.; Alloatti, L.; Wade, M. T.; Sun, C.; Kruger, S. A.; Meng, H.; Al Qubaisi, K.; Wang, I.; Zhang, B.; Khilo, A.; Baiocco, C. V.; Popović, M. A.; Stojanović, V. M.; Ram, R. J. Integrating Photonics with Silicon Nanoelectronics for the next Generation of Systems on a Chip. *Nature* **2018**, *556* (7701), 349−353.

(18) Collings, N.; Davey, T.; Christmas, J.; Chu, D.; Crossland, B. The Applications and Technology of Phase-Only Liquid Crystal on Silicon Devices. *J. Dispersion Technol.* **2011**, *7* (3), 112−119.
(19) Hosseini, P.; Wright, C. D.; Bhaskaran, H. An Optoelectronic Framework Enabled by Low-Dimensional Phase-Change Films. *Nature* **2014**, *511* (7508), 206−211.
(20) Van Kessel, P. F.; Hornbeck, L. J.; Meier, R. E.; Douglass, M. R. A MEMS-Based Projection Display. *Proc. IEEE* **1998**, *86* (8), 1687−1704.
(21) Poulton, C. V.; Yaacobi, A.; Cole, D. B.; Byrd, M. J.; Raval, M.; Vermeulen, D.; Watts, M. R. Coherent Solid-State LIDAR with Silicon Photonic Optical Phased Arrays. *Opt. Lett., OL* **2017**, *42* (20), 4091−4094.
(22) Poulton, C. V.; Byrd, M. J.; Russo, P.; Timurdogan, E.; Khandaker, M.; Vermeulen, D.; Watts, M. R. Long-Range LiDAR and Free-Space Data Communication With High-Performance Optical Phased Arrays. *IEEE J. Sel. Top. Quantum Electron* **2019**, *25* (5), 7700108.
(23) Miller, S. A.; Chang, Y.-C.; Phare, C. T.; Shin, M. C.; Zadka, M.; Roberts, S. P.; Stern, B.; Ji, X.; Mohanty, A.; Gordillo, O. A. J.; Dave, U. D.; Lipson, M. Large-Scale Optical Phased Array Using a Low-Power Multi-Pass Silicon Photonic Platform. *Optica, OPTICA* **2020**, *7* (1), 3−6.
(24) Zhang, X.; Kwon, K.; Henriksson, J.; Luo, J.; Wu, M. C. A Large-Scale Microelectromechanical-Systems-Based Silicon Photonics LiDAR. *Nature* **2022**, *603* (7900), 253−258.
(25) Watts, M. R.; Sun, J.; DeRose, C.; Trotter, D. C.; Young, R. W.; Nielson, G. N. Adiabatic Thermo-Optic Mach−Zehnder Switch. *Opt. Lett., OL* **2013**, *38* (5), 733−735.
(26) Zhuang, L.; Roeloffzen, C. G. H.; Hoekman, M.; Boller, K.-J.; Lowery, A. J. Programmable Photonic Signal Processor Chip for Radiofrequency Applications. *Optica, OPTICA* **2015**, *2* (10), 854−859.
(27) Zhang, W.; Yao, J. Photonic Integrated Field-Programmable Disk Array Signal Processor. *Nat. Commun.* **2020**, *11* (1), 406.
(28) Pérez, D.; Gasulla, I.; Crudgington, L.; Thomson, D. J.; Khokhar, A. Z.; Li, K.; Cao, W.; Mashanovich, G. Z.; Capmany, J. Multipurpose Silicon Photonics Signal Processor Core. *Nat. Commun.* **2017**, *8* (1), 636.
(29) Wu, C.; Yu, H.; Lee, S.; Peng, R.; Takeuchi, I.; Li, M. Programmable Phase-Change Metasurfaces on Waveguides for Multimode Photonic Convolutional Neural Network. *Nat. Commun.* **2021**, *12* (1), 96.
(30) Seok, T. J.; Quack, N.; Han, S.; Muller, R. S.; Wu, M. C. Large-Scale Broadband Digital Silicon Photonic Switches with Vertical Adiabatic Couplers. *Optica, OPTICA* **2016**, *3* (1), 64−70.
(31) Wang, Y.; Zhou, G.; Zhang, X.; Kwon, K.; Blanche, P.-A.; Triesault, N.; Yu, K.; Wu, M. C. 2D Broadband Beamsteering with Large-Scale MEMS Optical Phased Array. *Optica, OPTICA* **2019**, *6* (5), 557−562.
(32) Edinger, P.; Takabayashi, A. Y.; Errando-Herranz, C.; Khan, U.; Sattari, H.; Verheyen, P.; Bogaerts, W.; Quack, N.; Gylfason, K. B. Silicon Photonic Microelectromechanical Phase Shifters for Scalable Programmable Photonics. *Opt. Lett., OL* **2021**, *46* (22), 5671−5674.
(33) Gyger, S.; Zichi, J.; Schweickert, L.; Elshaari, A. W.; Steinhauer, S.; Covre da Silva, S. F.; Rastelli, A.; Zwiller, V.; Jöns, K. D.; Errando-Herranz, C. Reconfigurable Photonics with On-Chip Single-Photon Detectors. *Nat. Commun.* **2021**, *12* (1), 1408.
(34) Seok, T. J.; Kwon, K.; Henriksson, J.; Luo, J.; Wu, M. C. Wafer-Scale Silicon Photonic Switches beyond Die Size Limit. *Optica, OPTICA* **2019**, *6* (4), 490−494.
(35) Haffner, C.; Joerg, A.; Doderer, M.; Mayor, F.; Chelladurai, D.; Fedoryshyn, Y.; Roman, C. I.; Mazur, M.; Burla, M.; Lezec, H. J.; Aksyuk, V. A.; Leuthold, J. Nano−Opto-Electro-Mechanical Switches Operated at CMOS-Level Voltages. *Science* **2019**, *366* (6467), 860−864.
(36) Wuttig, M.; Yamada, N. Phase-Change Materials for Rewriteable Data Storage. *Nat. Mater.* **2007**, *6* (11), 824−832.
(37) Raoux, S.; Xiong, F.; Wuttig, M.; Pop, E. Phase Change Materials and Phase Change Memory. *MRS Bull.* **2014**, *39* (8), 703−710.
(38) Zhang, W.; Mazzarello, R.; Wuttig, M.; Ma, E. Designing Crystallization in Phase-Change Materials for Universal Memory and Neuro-Inspired Computing. *Nat. Rev. Mater.* **2019**, *4* (3), 150−168.
(39) Delaney, M.; Zeimpekis, I.; Lawson, D.; Hewak, D. W.; Muskens, O. L. A New Family of Ultralow Loss Reversible Phase-Change Materials for Photonic Integrated Circuits: Sb2S3 and Sb2Se3. *Adv. Funct. Mater.* **2020**, *30* (36), 2002447.
(40) Zheng, J.; Khanolkar, A.; Xu, P.; Colburn, S.; Deshmukh, S.; Myers, J.; Frantz, J.; Pop, E.; Hendrickson, J.; Doylend, J.; Boechler, N.; Majumdar, A. GST-on-Silicon Hybrid Nanophotonic Integrated Circuits: A Non-Volatile Quasi-Continuously Reprogrammable Platform. *Opt. Mater. Express, OME* **2018**, *8* (6), 1551−1561.
(41) Rios, C.; Hosseini, P.; Wright, C. D.; Bhaskaran, H.; Pernice, W. H. P. On-Chip Photonic Memory Elements Employing Phase-Change Materials. *Adv. Mater.* **2014**, *26* (9), 1372−1377.
(42) Fang, Z.; Zheng, J.; Saxena, A.; Whitehead, J.; Chen, Y.; Majumdar, A. Non-Volatile Reconfigurable Integrated Photonics Enabled by Broadband Low-Loss Phase Change Material. *Adv. Opt. Mater.* **2021**, *9* (9), 2002049.
(43) Wuttig, M.; Bhaskaran, H.; Taubner, T. Phase-Change Materials for Non-Volatile Photonic Applications. *Nat. Photonics* **2017**, *11* (8), 465−476.
(44) Zhang, Y.; Chou, J. B.; Li, J.; Li, H.; Du, Q.; Yadav, A.; Zhou, S.; Shalaginov, M. Y.; Fang, Z.; Zhong, H.; Roberts, C.; Robinson, P.; Bohlin, B.; Ríos, C.; Lin, H.; Kang, M.; Gu, T.; Warner, J.; Liberman, V.; Richardson, K.; Hu, J. Broadband Transparent Optical Phase Change Materials for High-Performance Nonvolatile Photonics. *Nat. Commun.* **2019**, *10* (1), 4279.
(45) Ríos, C.; Du, Q.; Zhang, Y.; Popescu, C.-C.; Shalaginov, M. Y.; Miller, P.; Roberts, C.; Kang, M.; Richardson, K. A.; Gu, T.; Vitale, S. A.; Hu, J. Ultra-Compact Nonvolatile Photonics Based on Electrically Reprogrammable Transparent Phase Change Materials. *arXiv:2105.06010 [physics.optics]* **2021**, na.
(46) Miscuglio, M.; Sorger, V. J. Photonic Tensor Cores for Machine Learning. *Appl. Phys. Rev.* **2020**, *7* (3), 031404.
(47) Zhang, Q.; Zhang, Y.; Li, J.; Soref, R.; Gu, T.; Hu, J. Broadband Nonvolatile Photonic Switching Based on Optical Phase Change Materials: Beyond the Classical Figure-of-Merit. *Opt. Lett., OL* **2018**, *43* (1), 94−97.
(48) Xu, P.; Zheng, J.; Doylend, J. K.; Majumdar, A. Low-Loss and Broadband Nonvolatile Phase-Change Directional Coupler Switches. *ACS Photonics* **2019**, *6* (2), 553−557.
(49) Chen, R.; Fang, Z.; Fröch, J. E.; Xu, P.; Zheng, J.; Majumdar, A. Broadband Nonvolatile Electrically Controlled Programmable Units in Silicon Photonics. *ACS Photonics* **2022**, *9* (6), 2142−2150.
(50) Wuttig, M.; Yamada, N. Phase-Change Materials for Rewriteable Data Storage. *Nat. Mater.* **2007**, *6* (11), 824−832.
(51) Pernice, W. H. P.; Bhaskaran, H. Photonic Non-Volatile Memories Using Phase Change Materials. *Appl. Phys. Lett.* **2012**, *101* (17), 171101.
(52) Ríos, C.; Stegmaier, M.; Hosseini, P.; Wang, D.; Scherer, T.; Wright, C. D.; Bhaskaran, H.; Pernice, W. H. P. Integrated All-Photonic Non-Volatile Multi-Level Memory. *Nat. Photonics* **2015**, *9* (11), 725−732.
(53) Wang, Q.; Rogers, E. T. F.; Gholipour, B.; Wang, C. M.; Yuan, G.; Teng, J.; Zheludev, N. I. Optically Reconfigurable Metasurfaces and Photonic Devices Based on Phase Change Materials. *Nat. Photonics* **2016**, *10* (1), 60−65.
(54) Cheng, Z.; Ríos, C.; Youngblood, N.; Wright, C. D.; Pernice, W. H. P.; Bhaskaran, H. Device-Level Photonic Memories and Logic Applications Using Phase-Change Materials. *Adv. Mater.* **2018**, *30* (32), 1802435.
(55) Li, X.; Youngblood, N.; Ríos, C.; Cheng, Z.; Wright, C. D.; Pernice, W. H.; Bhaskaran, H. Fast and Reliable Storage Using a 5 Bit, Nonvolatile Photonic Memory Cell. *Optica, OPTICA* **2019**, *6* (1), 1−6.


https://doi.org/10.1021/acsphotonics.2c00976
ACS Photonics XXXX, XXX, XXX−XXX

(56) Feldmann, J.; Youngblood, N.; Karpov, M.; Gehring, H.; Li, X.; Stappers, M.; Le Gallo, M.; Fu, X.; Lukashchuk, A.; Raja, A. S.; Liu, J.; Wright, C. D.; Sebastian, A.; Kippenberg, T. J.; Pernice, W. H. P.; Bhaskaran, H. Parallel Convolutional Processing Using an Integrated Photonic Tensor Core. *Nature* **2021**, *589* (7840), 52−58.
(57) Cheng, Z.; Ríos, C.; Pernice, W. H. P.; Wright, C. D.; Bhaskaran, H. On-Chip Photonic Synapse. *Sci. Adv.* **2017**, *3* (9), e1700160.
(58) Ríos, C.; Youngblood, N.; Cheng, Z.; Le Gallo, M.; Pernice, W. H. P.; Wright, C. D.; Sebastian, A.; Bhaskaran, H. In-Memory Computing on a Photonic Platform. *Sci. Adv.* **2019**, *5* (2), eaau5759.
(59) Wu, C.; Yang, X.; Yu, H.; Peng, R.; Takeuchi, I.; Chen, Y.; Li, M. Harnessing Optoelectronic Noises in a Photonic Generative Network. *Sci. Adv.* **2022**, *8* (3), eabm2956.
(60) Feldmann, J.; Stegmaier, M.; Gruhler, N.; Ríos, C.; Bhaskaran, H.; Wright, C. D.; Pernice, W. H. P. Calculating with Light Using a Chip-Scale All-Optical Abacus. *Nat. Commun.* **2017**, *8* (1), 1256.
(61) Michel, A. K. U.; Chigrin, D. N.; Maß, T. W. W.; Schönauer, K.; Salinga, M.; Wuttig, M.; Taubner, T. Using Low-Loss Phase-Change Materials for Mid-Infrared Antenna Resonance Tuning. *Nano Lett.* **2013**, *13* (8), 3470−3475.
(62) Abdollahramezani, S.; Hemmatyar, O.; Taghinejad, M.; Taghinejad, H.; Krasnok, A.; Eftekhar, A. A.; Teichrib, C.; Deshmukh, S.; El-Sayed, M. A.; Pop, E.; Wuttig, M.; Alù, A.; Cai, W.; Adibi, A. Electrically Driven Reprogrammable Phase-Change Metasurface Reaching 80% Efficiency. *Nat. Commun.* **2022**, *13* (1), 1696.
(63) Zhang, Y.; Fowler, C.; Liang, J.; Azhar, B.; Shalaginov, M. Y.; Deckoff-Jones, S.; An, S.; Chou, J. B.; Roberts, C. M.; Liberman, V.; Kang, M.; Ríos, C.; Richardson, K. A.; Rivero-Baleine, C.; Gu, T.; Zhang, H.; Hu, J. Electrically Reconfigurable Non-Volatile Metasurface Using Low-Loss Optical Phase-Change Material. *Nat. Nanotechnol.* **2021**, *16* (6), 661−666.
(64) Wang, Y.; Landreman, P.; Schoen, D.; Okabe, K.; Marshall, A.; Celano, U.; Wong, H. S. P.; Park, J.; Brongersma, M. L. Electrical Tuning of Phase-Change Antennas and Metasurfaces. *Nat. Nanotechnol.* **2021**, *16* (6), 667−672.
(65) Julian, M.; Williams, C.; Borg, S.; Bartram, S.; Kim, H. J. Reversible Optical Tuning of GeSbTe Phase-Change Metasurface Spectral Filters for Mid-Wave Infrared Imaging. *Optica* **2020**, *7* (7), 746−754.
(66) Shalaginov, M. Y.; An, S.; Zhang, Y.; Yang, F.; Su, P.; Liberman, V.; Chou, J. B.; Roberts, C. M.; Kang, M.; Rios, C.; Du, Q.; Fowler, C.; Agarwal, A.; Richardson, K. A.; Rivero-Baleine, C.; Zhang, H.; Hu, J.; Gu, T. Reconfigurable All-Dielectric Metalens with Diffraction-Limited Performance. *Nat. Commun.* **2021**, *12* (1), 1225.
(67) Dong, W.; Qiu, Y.; Zhou, X.; Banas, A.; Banas, K.; Breese, M. B. H.; Cao, T.; Simpson, R. E. Tunable Mid-Infrared Phase-Change Metasurface. *Adv. Opt. Mater.* **2018**, *6* (14), 1701346.
(68) Badloe, T.; Lee, J.; Seong, J.; Rho, J. Tunable Metasurfaces: The Path to Fully Active Nanophotonics. *Adv. Photonics Res.* **2021**, *2* (9), 2000205.
(69) Mikheeva, E.; Kyrou, C.; Bentata, F.; Khadir, S.; Cueff, S.; Genevet, P. Space and Time Modulations of Light with Metasurfaces: Recent Progress and Future Prospects. *ACS Photonics* **2022**, *9* (5), 1458−1482.
(70) Afridi, A.; Canet-Ferrer, J.; Philippet, L.; Osmond, J.; Berto, P.; Quidant, R. Electrically Driven Varifocal Silicon Metalens. *ACS Photonics* **2018**, *5* (11), 4497−4503.
(71) Colburn, S.; Zhan, A.; Majumdar, A. Varifocal Zoom Imaging with Large Area Focal Length Adjustable Metalenses. *Optica, OPTICA* **2018**, *5* (7), 825−831.
(72) Wang, Y.; Chen, L.; Tang, S.; Xu, P.; Ding, F.; Fang, Z.; Majumdar, A. Helicity-Dependent Continuous Varifocal Metalens Based on Bilayer Dielectric Metasurfaces. *Opt. Express, OE* **2021**, *29* (24), 39461.
(73) Wei, S.; Cao, G.; Lin, H.; Yuan, X.; Somekh, M.; Jia, B. A Varifocal Graphene Metalens for Broadband Zoom Imaging Covering the Entire Visible Region. *ACS Nano* **2021**, *15* (3), 4769−4776.
(74) Klopfer, E.; Dagli, S.; Barton, D., III; Lawrence, M.; Dionne, J. A. High-Quality-Factor Silicon-on-Lithium Niobate Metasurfaces for Electro-Optically Reconfigurable Wavefront Shaping. *Nano Lett.* **2022**, *22* (4), 1703−1709.
(75) Li, S. Q.; Xu, X.; Veetil, R. M.; Valuckas, V.; Paniagua-Domínguez, R.; Kuznetsov, A. I. Phase-Only Transmissive Spatial Light Modulator Based on Tunable Dielectric Metasurface. *Science* **2019**, *364* (6445), 1087−1090.
(76) Park, J.; Jeong, B. G.; Kim, S. I.; Lee, D.; Kim, J.; Shin, C.; Lee, C. B.; Otsuka, T.; Kyoung, J.; Kim, S.; Yang, K. Y.; Park, Y. Y.; Lee, J.; Hwang, I.; Jang, J.; Song, S. H.; Brongersma, M. L.; Ha, K.; Hwang, S. W.; Choo, H.; Choi, B. L. All-Solid-State Spatial Light Modulator with Independent Phase and Amplitude Control for Three-Dimensional LiDAR Applications. *Nat. Nanotechnol.* **2021**, *16* (1), 69−76.
(77) Mansha, S.; Moitra, P.; Xu, X.; Mass, T. W. W.; Veetil, R. M.; Liang, X.; Li, S.-Q.; Paniagua-Domínguez, R.; Kuznetsov, A. I. High Resolution Multispectral Spatial Light Modulators Based on Tunable Fabry-Perot Nanocavities. *Light Sci. Appl.* **2022**, *11* (1), 141.
(78) Li, L.; Jun Cui, T.; Ji, W.; Liu, S.; Ding, J.; Wan, X.; Bo Li, Y.; Jiang, M.; Qiu, C.-W.; Zhang, S. Electromagnetic Reprogrammable Coding-Metasurface Holograms. *Nat. Commun.* **2017**, *8* (1), 197.
(79) Li, J.; Kamin, S.; Zheng, G.; Neubrech, F.; Zhang, S.; Liu, N. Addressable Metasurfaces for Dynamic Holography and Optical Information Encryption. *Sci. Adv.* **2018**, *4* (6), eaar6768.
(80) Wu, C.; Yu, H.; Li, H.; Zhang, X.; Takeuchi, I.; Li, M. Low-Loss Integrated Photonic Switch Using Subwavelength Patterned Phase Change Material. *ACS Photonics* **2019**, *6* (1), 87−92.
(81) Delaney, M.; Zeimpekis, I.; Du, H.; Yan, X.; Banakar, M.; Thomson, D. J.; Hewak, D. W.; Muskens, O. L. Nonvolatile Programmable Silicon Photonics Using an Ultralow-Loss Sb2Se3 Phase Change Material. *Sci. Adv.* **2021**, *7* (25), eabg3500.
(82) Farmakidis, N.; Youngblood, N.; Li, X.; Tan, J.; Swett, J. L.; Cheng, Z.; Wright, C. D.; Pernice, W. H. P.; Bhaskaran, H. Plasmonic Nanogap Enhanced Phase-Change Devices with Dual Electrical-Optical Functionality. *Sci. Adv.* **2019**, *5* (11), eaaw2687.
(83) Zheng, J.; Fang, Z.; Wu, C.; Zhu, S.; Xu, P.; Doylend, J. K.; Deshmukh, S.; Pop, E.; Dunham, S.; Li, M.; Majumdar, A. Nonvolatile Electrically Reconfigurable Integrated Photonic Switch Enabled by a Silicon PIN Diode Heater. *Adv. Mater.* **2020**, *32* (31), 2001218.
(84) Kato, K.; Kuwahara, M.; Kawashima, H.; Tsuruoka, T.; Tsuda, H. Current-Driven Phase-Change Optical Gate Switch Using Indium−Tin-Oxide Heater. *Appl. Phys. Express* **2017**, *10* (7), 072201.
(85) Meng, J.; Peserico, N.; Ma, X.; Zhang, Y.; Popescu, C.-C.; Kang, M.; Miscuglio, M.; Richardson, K.; Hu, J.; Sorger, V. J. Electrical Programmable Low-Loss High Cyclable Nonvolatile Photonic Random-Access Memory. *arXiv.2203.13337* **2022**, na.
(86) Taghinejad, H.; Abdollahramezani, S.; Eftekhar, A. A.; Fan, T.; Hosseinnia, A. H.; Hemmatyar, O.; Eshaghian Dorche, A.; Gallmon, A.; Adibi, A. ITO-Based Microheaters for Reversible Multi-Stage Switching of Phase-Change Materials: Towards Miniaturized beyond-Binary Reconfigurable Integrated Photonics. *Opt. Express* **2021**, *29* (13), 20449−20462.
(87) Zhang, H.; Zhou, L.; Xu, J.; Wang, N.; Hu, H.; Lu, L.; Rahman, B. M. A.; Chen, J. Nonvolatile Waveguide Transmission Tuning with Electrically-Driven Ultra-Small GST Phase-Change Material. *Sci. Bull.* **2019**, *64* (11), 782−789.
(88) Ríos, C.; Zhang, Y.; Shalaginov, M.; Deckoff-Jones, S.; Wang, H.; An, S.; Zhang, H.; Kang, M.; Richardson, K. A.; Roberts, C.; Chou, J. B.; Liberman, V.; Vitale, S. A.; Kong, J.; Gu, T.; Hu, J. Multi-Level Electro-Thermal Switching of Optical Phase-Change Materials Using Graphene. *Adv. Photonics Res.* **2020**, *1* (2), 2000034.
(89) Fang, Z.; Chen, R.; Zheng, J.; Khan, A. I.; Neilson, K. M.; Geiger, S. J.; Callahan, D. M.; Moebius, M. G.; Saxena, A.; Chen, M. E.; Rios, C.; Hu, J.; Pop, E.; Majumdar, A. Ultra-Low-Energy Programmable Non-Volatile Silicon Photonics Based on Phase-Change Materials with Graphene Heaters. *Nat. Nanotechnol.* **2022**, *17* (8), 842−848.


https://doi.org/10.1021/acsphotonics.2c00976
ACS Photonics XXXX, XXX, XXX−XXX

(90) Youngblood, N.; Talagrand, C.; Porter, B. F.; Galante, C. G.; Kneepkens, S.; Triggs, G.; Ghazi Sarwat, S.; Yarmolich, D.; Bonilla, R. S.; Hosseini, P.; Taylor, R. A.; Bhaskaran, H. Reconfigurable Low-Emissivity Optical Coating Using Ultrathin Phase Change Materials. *ACS Photonics* **2022**, *9* (1), 90−100.
(91) Zheng, J.; Zhu, S.; Xu, P.; Dunham, S.; Majumdar, A. Modeling Electrical Switching of Nonvolatile Phase-Change Integrated Nanophotonic Structures with Graphene Heaters. *ACS Appl. Mater. Interfaces* **2020**, *12* (19), 21827−21836.
(92) Erickson, J. R.; Shah, V.; Wan, Q.; Youngblood, N.; Xiong, F. Designing Fast and Efficient Electrically Driven Phase Change Photonics Using Foundry Compatible Waveguide-Integrated Microheaters. *Opt. Express, OE* **2022**, *30* (8), 13673−13689.
(93) Wuttig, M.; Bhaskaran, H.; Taubner, T. Phase-Change Materials for Non-Volatile Photonic Applications. *Nat. Photonics* **2017**, *11* (8), 465−476.
(94) Abdollahramezani, S.; Hemmatyar, O.; Taghinejad, H.; Krasnok, A.; Kiarashinejad, Y.; Zandehshahvar, M.; Alù, A.; Adibi, A. Tunable Nanophotonics Enabled by Chalcogenide Phase-Change Materials. *Nanophotonics* **2020**, *9* (5), 1189−1241.
(95) Fang, Z.; Chen, R.; Zheng, J.; Majumdar, A. Non-Volatile Reconfigurable Silicon Photonics Based on Phase-Change Materials. *IEEE J. Sel. Top. Quantum Electron* **2021**, *28* (3), 8200317.
(96) Shen, Y.; Harris, N. C.; Skirlo, S.; Prabhu, M.; Baehr-Jones, T.; Hochberg, M.; Sun, X.; Zhao, S.; Larochelle, H.; Englund, D.; Soljacic, M. Deep Learning with Coherent Nanophotonic Circuits. *Nat. Photonics* **2017**, *11* (7), 441−446.
(97) Harris, N. C.; Steinbrecher, G. R.; Prabhu, M.; Lahini, Y.; Mower, J.; Bunandar, D.; Chen, C.; Wong, F. N. C.; Baehr-Jones, T.; Hochberg, M.; Lloyd, S.; Englund, D. Quantum Transport Simulations in a Programmable Nanophotonic Processor. *Nat. Photonics* **2017**, *11* (7), 447−452.
(98) Ikuma, Y.; Saiki, T.; Tsuda, H. Proposal of a Small Self-Holding 2×2 Optical Switch Using Phase-Change Material. IEICE Electron. *Express* **2008**, *5*, 442−445.
(99) Dong, W.; Liu, H.; Behera, J. K.; Lu, L.; Ng, R. J. H.; Sreekanth, K. V.; Zhou, X.; Yang, J. K. W.; Simpson, R. E. Wide Bandgap Phase Change Material Tuned Visible Photonics. *Adv. Funct. Mater.* **2019**, *29* (6), 1806181.
(100) Tuma, T.; Pantazi, A.; Le Gallo, M.; Sebastian, A.; Eleftheriou, E. Stochastic Phase-Change Neurons. *Nat. Nanotechnol.* **2016**, *11* (8), 693−699.
(101) Pérez-López, D.; López, A.; DasMahapatra, P.; Capmany, J. Multipurpose Self-Configuration of Programmable Photonic Circuits. *Nat. Commun.* **2020**, *11* (1), 6359.
(102) Teo, T. Y.; Krbal, M.; Mistrik, J.; Prikryl, J.; Lu, L.; Simpson, R. E. Comparison and Analysis of Phase Change Materials-Based Reconfigurable Silicon Photonic Directional Couplers. *Opt. Mater. Express* **2022**, *12* (2), 606−621.
(103) De Leonardis, F.; Soref, R.; Passaro, V. M. N.; Zhang, Y.; Hu, J. Broadband Electro-Optical Crossbar Switches Using Low-Loss Ge2Sb2Se4Te1 Phase Change Material. *J. Light. Technol.* **2019**, *37* (13), 3183−3191.
(104) Martin-Monier, L.; Popescu, C. C.; Ranno, L.; Mills, B.; Geiger, S.; Callahan, D.; Moebius, M.; Hu, J. Endurance of Chalcogenide Optical Phase Change Materials: A Review. *Opt. Mater. Express, OME* **2022**, *12* (6), 2145−2167.
(105) Kim, S.; Burr, G. W.; Kim, W.; Nam, S.-W. Phase-Change Memory Cycling Endurance. *MRS Bull.* **2019**, *44* (9), 710−714.
(106) Atwood, G. Phase-Change Materials for Electronic Memories. *Science* **2008**, *321* (5886), 210−211.
(107) Zhang, Y.; Ríos, C.; Shalaginov, M. Y.; Li, M.; Majumdar, A.; Gu, T.; Hu, J. Myths and Truths about Optical Phase Change Materials: A Perspective. *Appl. Phys. Lett.* **2021**, *118* (21), 210501.
(108) Ohshima, N. Crystallization of Germanium−Antimony−Tellurium Amorphous Thin Film Sandwiched between Various Dielectric Protective Films. *J. Appl. Phys.* **1996**, *79* (11), 8357−8363.
(109) Aggarwal, S.; Milne, T.; Farmakidis, N.; Feldmann, J.; Li, X.; Shu, Y.; Cheng, Z.; Salinga, M.; Pernice, W. H.; Bhaskaran, H. Antimony as a Programmable Element in Integrated Nanophotonics. *Nano Lett.* **2022**, *22* (9), 3532−3538.
(110) Stegmaier, M.; Ríos, C.; Bhaskaran, H.; Wright, C. D.; Pernice, W. H. P. Nonvolatile All-Optical 1 × 2 Switch for Chipscale Photonic Networks. *Adv. Opt. Mater.* **2017**, *5* (1), 1600346.
(111) Gosciniak, J. Ultra-Compact Nonvolatile Plasmonic Phase Change Modulators and Switches with Dual Electrical−Optical Functionality. *AIP Adv.* **2022**, *12* (3), 035321.
(112) Xu, X.; Ren, G.; Feleppa, T.; Liu, X.; Boes, A.; Mitchell, A.; Lowery, A. J. Self-Calibrating Programmable Photonic Integrated Circuits. *Nat. Photonics* **2022**, *16* (8), 595−602.
(113) Reck, M.; Zeilinger, A.; Bernstein, H. J.; Bertani, P. Experimental Realization of Any Discrete Unitary Operator. *Phys. Rev. Lett.* **1994**, *73* (1), 58−61.
(114) Lu, L.; Zhao, S.; Zhou, L.; Li, D.; Li, Z.; Wang, M.; Li, X.; Chen, J. 16 × 16 Non-Blocking Silicon Optical Switch Based on Electro-Optic Mach-Zehnder Interferometers. *Opt. Express, OE* **2016**, *24* (9), 9295.
(115) Wu, C.; Yang, X.; Yu, H.; Peng, R.; Takeuchi, I.; Chen, Y.; Li, M. Harnessing Optoelectronic Noises in a Photonic Generative Network. *Sci. Adv.* **2022**, *8* (3), eabm2956.
(116) Feldmann, J.; Youngblood, N.; Wright, C. D.; Bhaskaran, H.; Pernice, W. H. P. All-Optical Spiking Neurosynaptic Networks with Self-Learning Capabilities. *Nature* **2019**, *569* (7755), 208−214.
(117) Pérez, D.; Gasulla, I.; Capmany, J. Programmable Multifunctional Integrated Nanophotonics. *Nanophotonics* **2018**, *7* (8), 1351−1371.
(118) Harris, N. C.; Carolan, J.; Bunandar, D.; Prabhu, M.; Hochberg, M.; Baehr-Jones, T.; Fanto, M. L.; Smith, A. M.; Tison, C. C.; Alsing, P. M.; Englund, D. Linear Programmable Nanophotonic Processors. *Optica, OPTICA* **2018**, *5* (12), 1623−1631.
(119) Macho-Ortiz, A.; Pérez-López, D.; Capmany, J. Optical Implementation of 2 × 2 Universal Unitary Matrix Transformations. *Laser Photonics Rev.* **2021**, *15* (7), 2000473.
(120) Bogaerts, W.; Pérez, D.; Capmany, J.; Miller, D. A. B.; Poon, J.; Englund, D.; Morichetti, F.; Melloni, A. Programmable Photonic Circuits. *Nature* **2020**, *586* (7828), 207−216.
(121) LeCun, Y.; Boser, B.; Denker, J.; Henderson, D.; Howard, R.; Hubbard, W.; Jackel, L.Handwritten Digit Recognition with a Back-Propagation Network. In *Advances in Neural Information Processing Systems*; Touretzky, D.,, Ed.; Morgan-Kaufmann, 1989; Vol. *2*; pp 396−404.
(122) Munder, S.; Gavrila, D. M. An Experimental Study on Pedestrian Classification. *IEEE Trans. Pattern Anal. Mach. Intell.* **2006**, *28* (11), 1863−1868.
(123) Krizhevsky, A.; Sutskever, I.; Hinton, G. E. ImageNet Classification with Deep Convolutional Neural Networks. *Commun. ACM* **2017**, *60* (6), 84−90.
(124) Bengio, Y.; Ducharme, R.; Vincent, P.A Neural Probabilistic Language Model. In *Advances in Neural Information Processing Systems*; MIT Press, 2000; Vol. *13*; pp 1−7.
(125) Collobert, R.; Weston, J.A Unified Architecture for Natural Language Processing: Deep Neural Networks with Multitask Learning. *Proceedings of the 25th International Conference on Machine Learning, ICML '08*; Association for Computing Machinery: New York, NY, U.S.A., 2008; pp 160−167; DOI: 10.1145/1390156.1390177.
(126) Mikolov, T.; Sutskever, I.; Chen, K.; Corrado, G. S.; Dean, J.Distributed Representations of Words and Phrases and Their Compositionality. In *Advances in Neural Information Processing Systems*; Burges, C. J., Bottou, L., Welling, M., Ghahramani, Z., Weinberger, K. Q.,, Eds.; Curran Associates, Inc., 2013; Vol. *26*; pp 1−9.
(127) Isola, P.; Zhu, J.-Y.; Zhou, T.; Efros, A. A.Image-To-Image Translation With Conditional Adversarial Networks. *Proceedings of the IEEE Conference on Computer Vision and Pattern Recognition (CVPR)*, July 2017; IEEE; pp 1125−1134.
(128) Zhu, J.-Y.; Park, T.; Isola, P.; Efros, A. A.Unpaired Image-To-Image Translation Using Cycle-Consistent Adversarial Networks.


https://doi.org/10.1021/acsphotonics.2c00976
ACS Photonics XXXX, XXX, XXX−XXX

*Proceedings of the IEEE International Conference on Computer Vision (ICCV)*, October 2017; IEEE; pp 2223−2232.
(129) Karras, T.; Laine, S.; Aila, T.A Style-Based Generator Architecture for Generative Adversarial Networks. *Proceedings of the IEEE/CVF Conference on Computer Vision and Pattern Recognition (CVPR)*, June 2019; IEEE; pp 4401−4410.
(130) Lagaris, I. E.; Likas, A.; Fotiadis, D. I. Artificial Neural Networks for Solving Ordinary and Partial Differential Equations. *IEEE Trans. Neural Netw.* **1998**, *9* (5), 987−1000.
(131) Raissi, M.; Perdikaris, P.; Karniadakis, G. E. Physics-Informed Neural Networks: A Deep Learning Framework for Solving Forward and Inverse Problems Involving Nonlinear Partial Differential Equations. *J. Comput. Phys.* **2019**, *378*, 686−707.
(132) Sirignano, J.; Spiliopoulos, K. DGM: A Deep Learning Algorithm for Solving Partial Differential Equations. *J. Comput. Phys.* **2018**, *375*, 1339−1364.
(133) Vandoorne, K.; Mechet, P.; Van Vaerenbergh, T.; Fiers, M.; Morthier, G.; Verstraeten, D.; Schrauwen, B.; Dambre, J.; Bienstman, P. Experimental Demonstration of Reservoir Computing on a Silicon Photonics Chip. *Nat. Commun.* **2014**, *5* (1), 3541.
(134) Li, H.; Balamurugan, G.; Kim, T.; Sakib, M. N.; Kumar, R.; Rong, H.; Jaussi, J.; Casper, B. A 3-D-Integrated Silicon Photonic Microring-Based 112-Gb/s PAM-4 Transmitter With Nonlinear Equalization and Thermal Control. *IEEE J. Solid-State Circuits* **2021**, *56* (1), 19−29.
(135) Li, H.; Casper, B.; Balamurugan, G.; Sakib, M.; Sun, J.; Driscoll, J.; Kumar, R.; Jayatilleka, H.; Rong, H.; Jaussi, J. A 112 Gb/s PAM4 Silicon Photonics Transmitter with Microring Modulator and CMOS Driver. *J. Light. Technol.* **2020**, *38* (1), 131−138.
(136) Moazeni, S.; Lin, S.; Wade, M.; Alloatti, L.; Ram, R. J.; Popovic, M.; Stojanovic, V. A 40-Gb/s PAM-4 Transmitter Based on a Ring-Resonator Optical DAC in 45-Nm SOI CMOS. *IEEE J. Solid-State Circuits* **2017**, *52* (12), 3503−3516.
(137) Mohanty, A.; Li, Q.; Tadayon, M. A.; Roberts, S. P.; Bhatt, G. R.; Shim, E.; Ji, X.; Cardenas, J.; Miller, S. A.; Kepecs, A.; Lipson, M. Reconfigurable Nanophotonic Silicon Probes for Sub-Millisecond Deep-Brain Optical Stimulation. *Nat. Biomed. Eng.* **2020**, *4* (2), 223−231.
(138) Cheng, R.; Zou, C.-L.; Guo, X.; Wang, S.; Han, X.; Tang, H. X. Broadband On-Chip Single-Photon Spectrometer. *Nat. Commun.* **2019**, *10* (1), 4104.
(139) Momeni, B.; Hosseini, E. S.; Adibi, A. Planar Photonic Crystal Microspectrometers in Silicon-Nitride for the Visible Range. *Opt. Express, OE* **2009**, *17* (19), 17060−17069.
(140) Notaros, J.; Raval, M.; Notaros, M.; Watts, M. R. Integrated-Phased-Array-Based Visible-Light Near-Eye Holographic Projector. *2019 Conference on Lasers and Electro-Optics (CLEO)* **2019**, 1−2.
(141) Hepp, C.; Müller, T.; Waselowski, V.; Becker, J. N.; Pingault, B.; Sternschulte, H.; Steinmüller-Nethl, D.; Gali, A.; Maze, J. R.; Atatüre, M.; Becher, C. Electronic Structure of the Silicon Vacancy Color Center in Diamond. *Phys. Rev. Lett.* **2014**, *112* (3), 036405.
(142) Schirhagl, R.; Chang, K.; Loretz, M.; Degen, C. L. Nitrogen-Vacancy Centers in Diamond: Nanoscale Sensors for Physics and Biology. *Annu. Rev. Phys. Chem.* **2014**, *65* (1), 83−105.
(143) Arun, P.; Vedeshwar, A. G.; Mehra, N. C. Laser-Induced Crystallization In Sb2S3 Films. *Mater. Res. Bull.* **1997**, *32* (7), 907−913.
(144) Wilson, D. J.; Schneider, K.; Hönl, S.; Anderson, M.; Baumgartner, Y.; Czornomaz, L.; Kippenberg, T. J.; Seidler, P. Integrated Gallium Phosphide Nonlinear Photonics. *Nat. Photonics* **2020**, *14* (1), 57−62.
(145) Wan, N. H.; Lu, T.-J.; Chen, K. C.; Walsh, M. P.; Trusheim, M. E.; De Santis, L.; Bersin, E. A.; Harris, I. B.; Mouradian, S. L.; Christen, I. R.; Bielejec, E. S.; Englund, D. Large-Scale Integration of Artificial Atoms in Hybrid Photonic Circuits. *Nature* **2020**, *583* (7815), 226−231.
(146) Kim, J.-H.; Aghaeimeibodi, S.; Carolan, J.; Englund, D.; Waks, E. Hybrid Integration Methods for On-Chip Quantum Photonics. *Optica, OPTICA* **2020**, *7* (4), 291−308.
(147) Davis, K. M.; Miura, K.; Sugimoto, N.; Hirao, K. Writing Waveguides in Glass with a Femtosecond Laser. *Opt. Lett., OL* **1996**, *21* (21), 1729−1731.
(148) Sotillo, B.; Bharadwaj, V.; Hadden, J. P.; Sakakura, M.; Chiappini, A.; Fernandez, T. T.; Longhi, S.; Jedrkiewicz, O.; Shimotsuma, Y.; Criante, L.; Osellame, R.; Galzerano, G.; Ferrari, M.; Miura, K.; Ramponi, R.; Barclay, P. E.; Eaton, S. M. Diamond Photonics Platform Enabled by Femtosecond Laser Writing. *Sci. Rep.* **2016**, *6* (1), 35566.
(149) Meany, T.; Gräfe, M.; Heilmann, R.; Perez-Leija, A.; Gross, S.; Steel, M. J.; Withford, M. J.; Szameit, A. Laser Written Circuits for Quantum Photonics. *Laser Photonics Rev.* **2015**, *9* (4), 363−384.
(150) Dias, A.; Muñoz, F.; Alvarez, A.; Moreno-Zárate, P.; Atienzar, J.; Urbieta, A.; Fernandez, P.; Pardo, M.; Serna, R.; Solis, J. Femtosecond Laser Writing of Photonic Devices in Borate Glasses Compositionally Designed to Be Laser Writable. *Opt. Lett., OL* **2018**, *43* (11), 2523−2526.
(151) Valle, G. D.; Osellame, R.; Laporta, P. Micromachining of Photonic Devices by Femtosecond Laser Pulses. *J. Opt. A: Pure Appl. Opt.* **2009**, *11* (1), 013001.
(152) Juodkazis, S.; Mizeikis, V.; Misawa, H. Three-Dimensional Microfabrication of Materials by Femtosecond Lasers for Photonics Applications. *J. Appl. Phys.* **2009**, *106* (5), 051101.


https://doi.org/10.1021/acsphotonics.2c00976
*ACS Photonics* XXXX, XXX, XXX−XXX